Cosmology with High-redshift Galaxy Survey: Neutrino Mass and Inflation

Masahiro Takada[1], Eiichiro Komatsu[2] and Toshifumi Futamase[1]

[1]*Astronomical Institute, Tohoku University, Sendai 980-8578, Japan and*
[2]*Department of Astronomy, The University of Texas at Austin, Austin, TX 78712*

High-z galaxy redshift surveys open up exciting possibilities for precision determinations of neutrino masses and inflationary models. The high-z surveys are more useful for cosmology than low-z ones owing to much weaker non-linearities in matter clustering, redshift-space distortion and galaxy bias, which allows us to use the galaxy power spectrum down to the smaller spatial scales that are inaccessible by low-z surveys. We can then utilize the two-dimensional information of the linear power spectrum in angular and redshift space to measure the scale-dependent suppression of matter clustering due to neutrino free-streaming as well as the shape of the primordial power spectrum. To illustrate capabilities of high-z surveys for constraining neutrino masses and the primordial power spectrum, we compare three future redshift surveys covering 300 square degrees at $0.5 < z < 2$, $2 < z < 4$, and $3.5 < z < 6.5$. We find that, combined with the cosmic microwave background data expected from the Planck satellite, these surveys allow precision determination of the total neutrino mass with the projected errors of $\sigma(m_{\nu,\text{tot}}) = 0.059$, 0.043, and 0.025 eV, respectively, thus yielding a positive *detection* of the neutrino mass rather than an upper limit, as $\sigma(m_{\nu,\text{tot}})$ is smaller than the lower limits to the neutrino masses implied from the neutrino oscillation experiments, by up to a factor of 4 for the highest redshift survey. The accuracies of constraining the tilt and running index of the primordial power spectrum, $\sigma(n_s) = (3.8,\ 3.7,\ 3.0) \times 10^{-3}$ and $\sigma(\alpha_s) = (5.9,\ 5.7,\ 2.4) \times 10^{-3}$ at $k_0 = 0.05$ Mpc^{-1}, respectively, are smaller than the current uncertainties by more than an order of magnitude, which will allow us to discriminate between candidate inflationary models. In particular, the error on α_s from the future highest redshift survey is not very far away from the prediction of a class of simple inflationary models driven by a massive scalar field with self-coupling, $\alpha_s = -(0.8 - 1.2) \times 10^{-3}$.

I. INTRODUCTION

We are living in the golden age of cosmology. Various data sets from precision measurements of temperature and polarization anisotropy in the cosmic microwave background (CMB) radiation as well as those of matter density fluctuations in the large-scale structure of the universe mapped by galaxy redshift surveys, Lyman-α forests and weak gravitational lensing observations are in a spectacular agreement with the concordance ΛCDM model [1–4]. These results assure that theory of cosmological linear perturbations is basically correct, and can accurately describe the evolution of photons, neutrinos, baryons, and collisionless dark matter particles [5–7], for given initial perturbations generated during inflation [8, 9]. The predictions from linear perturbation theory can be compared with the precision cosmological measurements, in order to derive stringent constraints on the various basic cosmological parameters. Future observations with better sensitivity and higher precision will continue to further improve our understanding of the universe.

Fluctuations in different cosmic fluids (dark matter, photons, baryons, and neutrinos) imprint characteristic features in their power spectra, owing to their interaction properties, thermal history, equation of state, and speed of sound. A remarkable example is the acoustic oscillation in the photon-baryon fluid that was generated before the decoupling epoch of photons, $z \simeq 1088$, which has been observed in the power spectrum of CMB temperature anisotropy [10], temperature–polarization cross correlation [11], and distribution of galaxies [12, 13].

Yet, the latest observations have shown convincingly that we still do not understand much of the universe. The standard model of cosmology tells us that the universe has been dominated by four components. In chronological order the four components are: early dark energy (also known as "inflaton" fields), radiation, dark matter, and late-time dark energy. The striking fact is that we do not understand the precise nature of three (dark matter, and early and late-time dark energy) out of the four components; thus, understanding the nature of these three dark components has been and will continue to be one of the most important topics in cosmology in next decades. Of which, one might be hopeful that the next generation particle accelerators such as the Large Hadron Collider (coming on-line in 2007) would find some hints for the nature of dark matter particles. On the other hand, the nature of late-time dark energy, which was discovered by measurements of luminosity distance out to distant Type Ia supernovae [14, 15], is a complete mystery, and many people have been trying to find a way to constrain properties of dark energy (see, e.g., [16] for a review).

How about the early dark energy, inflaton fields, which caused the expansion of the universe to accelerate in the very early universe? We know little about the nature of inflaton, just like we know little about the nature of late-time dark energy. The required property of inflaton fields is basically the same as that of the late-time

dark energy component: both must have a large negative pressure which is less than $-1/3$ of their energy density. To proceed further, however, one needs more information from observations. Different inflation models make specific predictions for the shape of the power spectrum [8] (see also Appendix B) as well as for other statistical properties [17] of primordial perturbations. Therefore, one of the most promising ways to constrain the physics of inflation, hence the nature of early dark energy in the universe, is to determine the shape of the primordial power spectrum accurately from observations. For example, the CMB data from the Wilkinson Microwave Anisotropy Probe [1], combined with the large-scale structure data from the Two-Degree Field Galaxy Redshift Survey [18], have already ruled out one of the popular inflationary models driven by a self-interacting massless scalar field [19]. Understanding the physics of inflation better will likely provide an important implication for late-time dark energy.

"Radiation" in the universe at around the matter-radiation equality mainly consists of photons and neutrinos; however, neutrinos actually stop being radiation when their mean energy per particle roughly equals the temperature of the universe. The physics of neutrinos has been revolutionized over the last decade by solar, atmospheric, reactor, and accelerator neutrino experiments having provided strong evidence for finite neutrino masses via mixing between different neutrino flavors, the so-called neutrino oscillations [20–24]. These experiments are, however, only sensitive to mass square differences between neutrino mass eigenstates, implying $\Delta m_{21}^2 \simeq 7 \times 10^{-5}$ eV^2 and $\Delta m_{32}^2 \simeq 3 \times 10^{-3}$ eV^2; thus, the most fundamental quantity of neutrinos, the absolute mass, has not been determined yet. Cosmological neutrinos that are the relic of the cosmic thermal history have distinct influences on the structure formation. Their large energy density, comparable to the energy density of photons before the matter-radiation equality, determines the expansion history of the universe. Even after the matter-radiation equality, neutrinos having become non-relativistic affect the structure formation by suppressing the growth of matter density fluctuations at small spatial scales owing to their large velocity dispersion [25, 26, 29, 30] (see Sec. II and Appendix A for more details). Therefore, the galaxy redshift surveys, combined with the CMB data, provide a powerful, albeit indirect, means to constraining the neutrino properties [31–35]. This approach also complements the theoretical and direct experimental efforts for understanding the neutrino physics. In fact, the cosmological constraints have placed the most stringent upper bound on the total neutrino mass, $m_{\nu,\mathrm{tot}} \lesssim 0.6\,\mathrm{eV}$ (2σ) [36], stronger than the direct experiment limit $\lesssim 2\,\mathrm{eV}$ [37]. In addition, the result obtained from the Liquid Scintillator Neutrino Detector (LSND) experiment, which implies $\bar{\nu}_\mu$ to $\bar{\nu}_e$ oscillations with $\Delta m^2 \gtrsim 0.2\,\mathrm{eV}^2$ [38] in an apparent contradiction with the other neutrino oscillation experiments mentioned above, potentially suggests the need for new physics: the cosmological observations will provide independent tests of this hypothesis.

In this paper we shall study the capability of future galaxy surveys at high redshifts, combined with the CMB data, for constraining (1) the neutrino properties, more specifically the total neutrino mass, $m_{\nu,\mathrm{tot}}$, and the number of non-relativistic neutrino species, N_ν^{nr}, and (2) the shape of the primordial power spectrum that is parameterized in terms of the spectral tilt, n_s, and the running index, α_s, motivated by inflationary predictions (see Appendix B). For the former, we shall pay particular attention to our ability to simultaneously constrain $m_{\nu,\mathrm{tot}}$ and N_ν^{nr}, as they will provide important clues to resolving the absolute mass scale as well as the neutrino mass hierarchy. The accuracy of determining the neutrino parameters and the power spectrum shape parameters will be derived using the Fisher information matrix formalism, including marginalization over the other cosmological parameters as well as the galaxy bias.

Our analysis differs from the previous work on the neutrino parameters in that we fully take into account the two-dimensional nature of the galaxy power spectrum in the line-of-sight and transverse directions, while the previous work used only spherically averaged, one-dimensional power spectra. The geometrical distortion due to cosmology and the redshift space distortion due to the peculiar velocity field will cause anisotropic features in the galaxy power spectrum. These features help to lift degeneracies between cosmological parameters, substantially reducing the uncertainties in the parameter determinations. This is especially true when variations in parameters of interest cause modifications in the power spectrum shape, which is indeed the case for the neutrino parameters, tilt and running index. The usefulness of the two-dimensional power spectrum, especially for high-redshift galaxy surveys, has been carefully investigated in the context of the prospected constraints on late-time dark energy properties [39–45].

We shall show the parameter forecasts for future wide-field galaxy surveys that are already being planned or seriously under consideration: the Fiber Multiple Object Spectrograph (FMOS) on Subaru telescope [46], its significantly expanded version, WFMOS [47], the Hobby–Ebery Telescope Dark Energy eXperiment (HETDEX) [48], and the Cosmic Inflation Probe (CIP) mission [49]. To model these surveys, we consider three hypothetical galaxy surveys which probe the universe over different ranges of redshift, (1) $0.5 \leq z \leq 2$, (2) $2 \leq z \leq 4$ and (3) $3.5 \leq z \leq 6.5$. We fix the sky coverage of each survey at $\Omega_s = 300$ deg^2 in order to make a fair comparison between different survey designs. As we shall show below, high-redshift surveys are extremely powerful for precision cosmology because they allow us to probe the linear power spectrum down to smaller length scales than surveys at low redshifts, protecting the cosmological information against systematics due to non-linear perturbations.

We shall also study how the parameter uncertainties

are affected by changes in the number density of sampled galaxies and the survey volume. The results would give us a good guidance to defining the optimal survey design to achieve the desired accuracies in parameter determinations.

The structure of this paper is as follows. In Sec. II, we review the physical pictures as to how the non-relativistic (massive) neutrinos lead to scale-dependent modifications in the growth of mass clustering relative to the pure CDM model. Sec. III defines the parameterization of the primordial power spectrum motivated by inflationary predictions. In Sec. IV we describe a methodology to model the galaxy power spectrum observable from a redshift survey that includes the two-dimensional nature in the line-of-sight and transverse directions. We then present the Fisher information matrix formalism that is used to estimate the projected uncertainties in the cosmological parameter determination from statistical errors on the galaxy power spectrum measurement for a given survey. After survey parameters are defined in Sec. V, we show the parameter forecasts in Sec. VI. Finally, we present conclusions and some discussions in Sec. VII. We review the basic properties of cosmological neutrinos in Appendix A, the basic predictions from inflationary models for the shape of the primordial power spectrum in Appendix B, and the relation between the primordial power spectrum and the observed power spectrum of matter density fluctuations in Appendix C.

In the following, we assume an adiabatic, cold dark matter (CDM) dominated cosmological model with flat geometry, which is supported by the WMAP results [1, 36], and employ the the notation used in [51, 52]: the present-day density of CDM, baryons, and non-relativistic neutrinos, in units of the critical density, are denoted as $\Omega_{\rm c}$, $\Omega_{\rm b}$, and Ω_ν, respectively. The total matter density is then $\Omega_{\rm m} = \Omega_{\rm c} + \Omega_{\rm b} + \Omega_\nu$, and f_ν is the ratio of the massive neutrino density contribution to $\Omega_{\rm m}$: $f_\nu = \Omega_\nu/\Omega_{\rm m}$.

II. NEUTRINO EFFECT ON STRUCTURE FORMATION

Throughout this paper we assume the standard thermal history in the early universe: there are three neutrino species with temperature equal to $(4/11)^{1/3}$ of the photon temperature. We then assume that $0 \leq N_\nu^{\rm nr} \leq 3$ species are massive and could become non-relativistic by the present epoch, and those non-relativistic neutrinos have equal masses, m_ν. As we show in Appendix A, the density parameter of the non-relativistic neutrinos is given by $\Omega_\nu h^2 = N_\nu^{\rm nr} m_\nu/(94.1\,{\rm eV})$, where we have assumed $2.725\,{\rm K}$ for the CMB temperature today [50], and h is the Hubble parameter defined as $H_0 = 100\,h\,{\rm km\,s^{-1}\,Mpc^{-1}}$. The neutrino mass fraction is thus given by

$$f_\nu \equiv \frac{\Omega_\nu}{\Omega_{\rm m}} = 0.05 \left(\frac{N_\nu^{\rm nr} m_\nu}{0.658\,{\rm eV}} \right) \left(\frac{0.14}{\Omega_{\rm m} h^2} \right). \quad (1)$$

Structure formation is modified by non-relativistic neutrinos on scales below the Hubble horizon size when the neutrinos became non-relativistic, $k_{\rm nr} = 0.0145(m_\nu/1\,{\rm eV})^{1/2}\Omega_{\rm m}^{1/2} h\,{\rm Mpc^{-1}}$ (see Eq. [A8]). In particular, the characteristic scale imprinted onto the galaxy power spectrum at a given redshift z is the neutrino free-streaming scale, which is defined by Eq. (A11):

$$k_{\rm fs}(z) = 0.113\,{\rm Mpc^{-1}} \left(\frac{m_\nu}{1\,{\rm eV}} \right) \left(\frac{\Omega_{\rm m} h^2}{0.14} \frac{5}{1+z} \right)^{1/2}. \quad (2)$$

Therefore, non-relativistic neutrinos with lighter masses suppress the growth of structure formation on larger spatial scales at a given redshift, and the free-streaming length becomes shorter at a lower redshift as neutrino velocity decreases with redshift. The most important property of the free-streaming scale is that it depends on the mass of each species, m_ν, rather than the total mass, $N_\nu^{\rm nr} m_\nu$; thus, measurements of $k_{\rm fs}$ allow us to distinguish different neutrino mass hierarchy models. Fortunately, $k_{\rm fs}$ appears on the scales that are accessible by galaxy surveys: $k_{\rm fs} = 0.096 - 0.179\,{\rm Mpc^{-1}}$ at $z = 6 - 1$ for $m_\nu = 1\,{\rm eV}$.

On the spatial scales larger than the free-streaming length, $k < k_{\rm fs}$, neutrinos can cluster and fall into gravitational potential well together with CDM and baryonic matter. In this case, perturbations in all matter components (CDM, baryon and neutrinos, denoted as 'cbν' hereafter) grow at the same rate given by

$$D_{\rm cb\nu}(k, z) \propto D(z) \qquad k \ll k_{\rm fs}(z), \quad (3)$$

where $D(z)$ is the usual linear growth factor (see, e.g., Eq. (4) in [53]). On the other hand, on the scales smaller than the free-streaming length, $k > k_{\rm fs}$, perturbations in non-relativistic neutrinos are absent due to the large velocity dispersion. In this case, the gravitational potential well is supported only by CDM and baryonic matter, and the growth of matter perturbations is slowed down relative to that on the larger scales. As a result, the matter power spectrum for $k > k_{\rm fs}$ is suppressed relative to that for $k < k_{\rm fs}$. In this limit the total matter perturbations grow at the slower rate given by

$$D_{\rm cb\nu}(k, z) \propto (1 - f_\nu)[D(z)]^{1-p} \qquad k \gg k_{\rm fs}(z), \quad (4)$$

where $p \equiv (5 - \sqrt{25 - 24 f_\nu})/4$ [25]. In [51, 52] an accurate fitting function for the scale-dependent growth rate was derived by matching these two asymptotic solutions. We shall use the fitting function throughout this paper.

Figure 1 shows suppression in the growth rate of total matter perturbations at $k = 0.01$, 0.1, and $1\,h{\rm Mpc^{-1}}$ due to the neutrino free-streaming. The suppression becomes more significant at lower redshifts for a given wavenumber, or for higher frequency perturbations at a given redshift, because neutrino can grow together with CDM and baryonic matter after the spatial scale of a given perturbation has become larger than the neutrino free-streaming scale that varies with redshift as given by
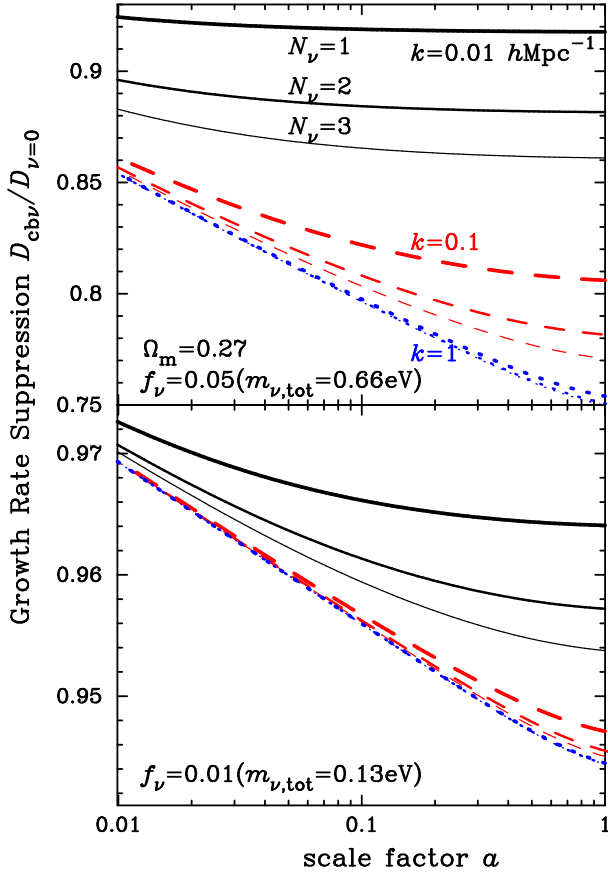
FIG. 1: Suppression in the growth rate of total matter perturbations (CDM, baryons and non-relativistic neutrinos), $D_{cb\nu}(a)$, due to neutrino free-streaming. ($a = (1+z)^{-1}$ is the scale factor.) *Upper panel*: $D_{cb\nu}(a)/D_{\nu=0}(a)$ for the neutrino mass fraction of $f_\nu = \Omega_\nu/\Omega_m = 0.05$. The number of non-relativistic neutrino species is varied from $N_\nu^{nr} = 1$, 2, and 3 (from thick to thin lines), respectively. The solid, dashed, and dotted lines represent $k = 0.01$, 0.1, and 1 hMpc^{-1}, respectively. *Lower panel*: $D_{cb\nu}(a)/D_{\nu=0}(a)$ for a smaller neutrino mass fraction, $f_\nu = 0.01$. Note that the total mass of non-relativistic neutrinos is fixed to $m_{\nu,\mathrm{tot}} = N_\nu^{nr} m_\nu = 0.66$ eV and 0.13 eV in the upper and lower panels, respectively.

Eq. (2). It is thus expected that a galaxy survey with different redshift slices can be used to efficiently extract the neutrino parameters, N_ν^{nr} and m_ν.

The upper and middle panels of Figure 2 illustrate how free-streaming of non-relativistic neutrinos suppresses the amplitude of linear matter power spectrum, $P(k)$, at $z = 4$. Note that we have normalized the primordial power spectrum such that all the power spectra match at $k \to 0$ (see § III). To illuminate the dependence of $P(k)$ on m_ν, we fix the total mass of non-relativistic neutrinos, $N_\nu^{nr} m_\nu$, by $f_\nu = 0.05$ and 0.01 in the upper and middle panels, respectively, and vary the number of non-relativistic neutrino species as $N_\nu^{nr} = 1$, 2 and 3. The suppression of power is clearly seen as one goes from $k < k_{fs}(z)$ to $k > k_{fs}(z)$ (see Eq. [2] for the value of k_{fs}). The way the power is suppressed may be easily understood by the dependence of $k_{fs}(z)$ on m_ν; for example,
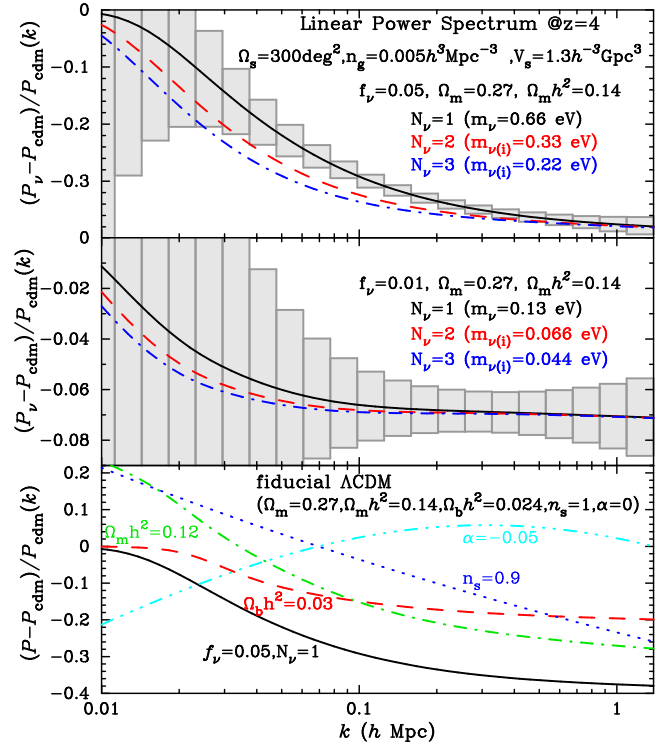

FIG. 2: *Upper panel*: A fractional suppression of power in the linear power spectrum at $z = 4$ due to free-streaming of non-relativistic neutrinos. We fix the total mass of non-relativistic neutrinos by $f_\nu = \Omega_\nu/\Omega_m = 0.05$, and vary the number of non-relativistic neutrino species (which have equal masses, m_ν) as $N_\nu^{nr} = 1$ (solid), 2 (dashed), and 3 (dot-dashed). The mass of individual neutrino species therefore varies as $m_\nu = 0.66$, 0.33, and 0.22 eV, respectively (see Eq. [1]). The shaded regions represent the 1-σ measurement errors on $P(k)$ in each k-bin, expected from a galaxy redshift survey observing galaxies at $3.5 \leq z \leq 4.5$ (see Table I for definition of the survey). Note that the errors are for the spherically averaged power spectrum over the shell of k in each bin. Different N_ν^{nr} could be discriminated in this case. *Middle panel*: Same as in the upper panel, but for a smaller neutrino mass fraction, $f_\nu = 0.01$. While it is not possible to discriminate between different N_ν^{nr}, the overall suppression on small scales is clearly seen. *Lower panel*: Dependences of the shape of $P(k)$ on the other cosmological parameters.

$P(k)$ at smaller k is more suppressed for a smaller m_ν, as lighter neutrinos have longer free-streaming lengths. On very small scales, $k \gg k_{fs}(z)$ ($k \gtrsim 1$ and $0.1\,\mathrm{Mpc}^{-1}$ for $f_\nu = 0.05$ and 0.01, respectively), however, the amount of suppression becomes nearly independent of k, and depends only on f_ν (or the total neutrino mass, $N_\nu^{nr} m_\nu$) as

$$\left|\frac{\Delta P}{P}\right| \approx 2f_\nu \left[1 + \frac{3\ln(D_{z=4})}{5}\right] \approx 8f_\nu. \quad (5)$$

We therefore conclude that one can extract f_ν and N_ν^{nr} separately from the shape of $P(k)$, if the suppression "pattern" in different regimes of k is accurately measured from observations.

Are observations good enough? The shaded boxes in the upper and middle panels in Figure 2 represent the 1-σ measurement errors on $P(k)$ expected from one of the fiducial galaxy surveys outlined in Sec. V. We find that $P(k)$ will be measured with $\sim 1\%$ accuracy in each k bin. If other cosmological parameters were perfectly known, the total mass of non-relativistic neutrinos as small as $m_{\nu,\text{tot}} = N_\nu^{\text{nr}} m_\nu \gtrsim 0.001\,\text{eV}$ would be detected at more than 2-σ. This limit is much smaller than the lower mass limit implied from the neutrino oscillation experiments, $0.06\,\text{eV}$. This estimate is, of course, unrealistic because a combination of other cosmological parameters could mimic the N_ν^{nr} or f_ν dependence of $P(k)$. The lower panel in Figure 2 illustrates how other cosmological parameters change the shape of $P(k)$. In the following, we shall extensively study how well future high-redshift galaxy surveys, combined with the cosmic microwave background data, can determine the mass of non-relativistic neutrinos and discriminate between different N_ν^{nr}, fully taking into account degeneracies between cosmological parameters.

III. SHAPE OF PRIMORDIAL POWER SPECTRUM AND INFLATIONARY MODELS

Inflation generally predicts that the primordial power spectrum of curvature perturbations is nearly scale-invariant. Different inflationary models make specific predictions for *deviations* of the primordial spectrum from a scale-invariant spectrum, and the deviation is often parameterized by the "tilt", n_s, and the "running index", α_s, of the primordial power spectrum. As the primordial power spectrum is nearly scale-invariant, $|n_s - 1|$ and $|\alpha_s|$ are predicted to be much less than unity.

This, however, does not mean that the observed matter power spectrum is also nearly scale-invariant. In Appendix C, we derive the power spectrum of total matter perturbations that is normalized by the primordial curvature perturbation (see Eq. [C6])

$$
\begin{aligned}
\frac{k^3 P(k,z)}{2\pi^2} &= \delta_{\mathcal{R}}^2 \left(\frac{2k^2}{5H_0^2 \Omega_{\text{m}}}\right)^2 \\
&\times D_{cb\nu}^2(k,z) T^2(k) \left(\frac{k}{k_0}\right)^{-1+n_s+\frac{1}{2}\alpha_s \ln(k/k_0)},
\end{aligned} \quad (6)
$$

where $k_0 = 0.05$ Mpc^{-1}, $\delta_{\mathcal{R}}^2 = 2.95 \times 10^{-9} A$, and A is the normalization parameter given by the WMAP collaboration [1]. We adopt $A = 0.871$, which gives $\delta_{\mathcal{R}} = 5.07 \times 10^{-5}$. (In the notation of [63, 64] $\delta_{\mathcal{R}} = \delta_\zeta$.) The linear transfer function, $T(k)$, describes the evolution of the matter power spectrum during radiation era and the interaction between photons and baryons before the decoupling of photons. Note that $T(k)$ depends only on non-inflationary parameters such as $\Omega_m h^2$ and Ω_b/Ω_m, and is independent of n_s and α_s. Also, the effects of non-relativistic neutrinos are captured in $D_{cb\nu}(k,z)$; thus, $T(k)$ is independent of time after the decoupling

epoch. We use the fitting function found in [51, 52] for $T(k)$. Note that the transfer function and the growth rate are normalized such that $T(k) \to 1$ and $D_{cb\nu}/a \to 1$ as $k \to 0$ during the matter era.

In Appendix B we describe generic predictions on n_s and α_s from inflationary models. For example, inflation driven by a massive, self-interacting scalar field predicts $n_s = 0.94 - 0.96$ and $\alpha_s = (0.8 - 1.2) \times 10^{-3}$ for the number of e-foldings of expansion factor before the end of inflation of 50. This example shows that precision determination of n_s and α_s allows us to discriminate between candidate inflationary models (see [8] for more details).

IV. MODELING GALAXY POWER SPECTRUM

A. Geometrical and Redshift-Space Distortion

Suppose now that we have a redshift survey of galaxies at some redshift. Galaxies are biased tracers of the underlying gravitational field, and the galaxy power spectrum measures how clustering strength of galaxies varies as a function of 3-dimensional wavenumbers, k (or the inverse of 3-dimensional length scales).

We do not measure the length scale directly in real space; rather, we measure (1) angular positions of galaxies on the sky, and (2) radial positions of galaxies in redshift space. To convert (1) and (2) to positions in 3-dimensional space, however, one needs to assume a reference cosmological model, which might be different from the true cosmology. An incorrect mapping of observed angular and redshift positions to 3-dimensional positions produces a distortion in the measured power spectrum, known as the "geometrical distortion" [54–56]. The geometrical distortion can be described as follows. The comoving size of an object at redshift z in radial, $r_\parallel$, and transverse, $r_\perp$, directions are computed from the extension in redshift, Δz, and the angular size, $\Delta\theta$, respectively, as

$$
\begin{aligned}
r_\parallel &= \frac{\Delta z}{H(z)}, \\
r_\perp &= D_A(z)\Delta\theta,
\end{aligned} \quad (7)
$$

where D_A is the comoving angular diameter distance given in the spatial sector of the Friedmann-Robertson-Walker line element, $dl^2 = a^2(d\chi^2 + D_A^2 d\Omega)$ (χ is the comoving radial distance). We assume a flat universe throughout this paper, in which case $\chi = D_A$. The comoving angular distance out to a galaxy at redshift z is

$$
D_A(z) = \int_0^z \frac{dz'}{H(z')}, \quad (8)
$$

where $H(z)$ is the Hubble parameter given by

$$
H^2(z) = H_0^2 \left[\Omega_{\text{m}}(1+z)^3 + \Omega_\Lambda\right]. \quad (9)
$$

Here $\Omega_m + \Omega_\Lambda = 1$, and $\Omega_\Lambda \equiv \Lambda/(3H_0^2)$ is the present-day density parameter of a cosmological constant, Λ. A tricky part is that $H(z)$ and $D_A(z)$ in Eq. (7) depend on cosmological models. It is therefore necessary to assume some fiducial cosmological model to compute the conversion factors. In the following, quantities in the fiducial cosmological model are distinguished by the subscript 'fid'. Then, the length scales in Fourier space in radial, $k_{\mathrm{fid}\|}$, and transverse, $k_{\mathrm{fid}\perp}$, directions are estimated from the inverse of $r_{\mathrm{fid}\|}$ and $r_{\mathrm{fid}\perp}$. These fiducial wavenumbers are related to the true wavenumbers by

$$
\begin{aligned}
k_\perp &= \frac{D_A(z)_{\mathrm{fid}}}{D_A(z)} k_{\mathrm{fid}\perp}, \\
k_\| &= \frac{H(z)}{H(z)_{\mathrm{fid}}} k_{\mathrm{fid}\|}.
\end{aligned}
\tag{10}
$$

Therefore, any difference between the fiducial cosmological model and the true model would cause anisotropic distortions in the estimated power spectrum in ($k_{\mathrm{fid}\perp}$, $k_{\mathrm{fid}\|}$) space.

In addition, shifts in z due to peculiar velocities of galaxies distort the shape of the power spectrum along the line-of-sight direction, which is known as the "redshift space distortion" [57]. From azimuthal symmetry around the line-of-sight direction, which is valid when a distant-observer approximation holds, the linear power spectrum estimated in redshift space, $P_s(k_{\mathrm{fid}\perp}, k_{\mathrm{fid}\|})$, is modeled in [39] as

$$
\begin{aligned}
P_s(k_{\mathrm{fid}\perp}, k_{\mathrm{fid}\|}) &= \frac{D_A(z)_{\mathrm{fid}}^2 H(z)}{D_A(z)^2 H(z)_{\mathrm{fid}}} \left[1 + \beta(k,z)\frac{k_\|^2}{k_\perp^2 + k_\|^2}\right]^2 \\
&\quad \times b_1^2 P(k,z),
\end{aligned}
\tag{11}
$$

where $k = (k_\perp^2 + k_\|^2)^{1/2}$ and

$$
\beta(k,z) \equiv -\frac{1}{b_1}\frac{d\ln D_{\mathrm{cb}\nu}(k,z)}{d\ln(1+z)},
\tag{12}
$$

is a function characterizing the linear redshift space distortion, and b_1 is a scale-independent, linear bias parameter. Note that $\beta(k,z)$ depends on both redshift and wavenumber via the linear growth rate. In the infall regime, $k \ll k_{\mathrm{fs}}(z)$, we have $b_1\beta(k,z) \approx -d\ln D(z)/d\ln(1+z)$, while in the free-streaming regime, $k \gg k_{\mathrm{fs}}(z)$, we have $b_1\beta(k,z) \approx -(1-p)d\ln D(z)/d\ln(1+z)$, where p is defined below Eq. (4).

One might think that the geometrical and redshift-space distortion effects are somewhat degenerate in the measured power spectrum. This would be true only if the power spectrum was a simple power law. Fortunately, characteristic, non-power-law features in $P(k)$ such as the broad peak from the matter-radiation equality, scale-dependent suppression of power due to baryons and non-relativistic neutrinos, the tilt and running of the primordial power spectrum, the baryonic acoustic oscillations, etc., help break degeneracies quite efficiently [39–44, 47, 55, 56].

B. Comments on Baryonic Oscillations

In this paper, we employ the linear transfer function with baryonic oscillations *smoothed out* (but includes non-relativistic neutrinos) [51, 52]. As extensively investigated in [39, 44, 47], the baryonic oscillations can be used as a standard ruler, thereby allowing one to precisely constrain $H(z)$ and $D_A(z)$ separately through the geometrical distortion effects (especially for a high-redshift survey). Therefore, our ignoring the baryonic oscillations might underestimate the true capability of redshift surveys for constraining cosmological parameters.

We have found that the constraints on n_s and α_s from galaxy surveys improve by a factor of 2–3 when baryonic oscillations are included. This is because the baryonic oscillations basically fix the values of Ω_m, $\Omega_m h^2$ and $\Omega_b h^2$, lifting parameter degeneracies between $\Omega_m h^2$, $\Omega_b h^2$, n_s, and α_s. However, we suspect that this is a rather optimistic forecast, as we are assuming a flat universe dominated by a cosmological constant. This might be a too strong prior, and relaxing our assumptions about geometry of the universe or the properties of dark energy will likely result in different forecasts for n_s and α_s. In this paper we try to separate the issues of non-flat universe and/or equation of state of dark energy from the physics of neutrinos and inflation. We do not include the baryonic oscillations in our analysis, in order to avoid too optimistic conclusions about the constraints on the neutrino parameters, n_s, and α_s.

Eventually, the full analysis including non-flat universe, arbitrary dark energy equation of state and its time dependence, non-relativistic neutrinos, n_s, and α_s, using all the information we have at hand including the baryonic oscillations, will be necessary. We leave it for a future publication (Takada and Komatsu, in preparation).

C. Parameter Forecast: Fisher Matrix Analysis

In order to investigate how well one can constrain the cosmological parameters for a given redshift survey design, one needs to specify measurement uncertainties of the galaxy power spectrum. When non-linearity is weak, it is reasonable to assume that observed density perturbations obey Gaussian statistics. In this case, there are two sources of statistical errors on a power spectrum measurement: the sampling variance (due to the limited number of independent wavenumbers sampled from a finite survey volume) and the shot noise (due to the imperfect sampling of fluctuations by the finite number of galaxies). To be more specific, the statistical error is given in [58, 59] by

$$
\left[\frac{\Delta P_s(k_i)}{P_s(k_i)}\right]^2 = \frac{2}{N_k}\left[1 + \frac{1}{\bar{n}_g P_s(k_i)}\right]^2,
\tag{13}
$$

where $\bar{n}_g$ is the mean number density of galaxies and N_k is the number of independent $\mathbf{k}_{\mathrm{fid}}$ modes within a given

bin at $k_{fid} = k_i$:

$$N_k = 2\pi k^2 \Delta k \Delta \mu \left(\frac{2\pi}{V_s^{1/3}} \right)^{-3}. \quad (14)$$

Here $2\pi/V_s^{1/3}$ is the size of the fundamental cell in k space, V_s is the comoving survey volume, and μ is the cosine of the angle between $\boldsymbol{k}_{fid}$ and the line-of-sight. Note that we have assumed that the galaxy selection function is uniform over the redshift slice we consider and ignored any boundary effects of survey geometry for simplicity.

The first term in Eq. (13) represents sampling variance. Errors become independent of the number density of galaxies when sampling variance dominates (i.e., $P_s \gg \bar{n}_g$ over the range of k considered), and thus the only way to reduce the errors is to survey a larger volume. On the other hand, the second term represents shot noise, which comes from discreteness of galaxy samples. When shot noise dominates ($P_s \ll \bar{n}_g$), the most effective way to reduce noise is to increase the number density of galaxies by increasing exposure time per field. Note that for a fixed $\bar{n}_g$ the relative importance of shot noise contribution can be suppressed by using galaxies with larger bias parameters, b_1, as $P_s \propto b_1^2$. In Sec. V we shall discuss more about the survey design that is required to attain the desired parameter accuracy.

We use the Fisher information matrix formalism to convert the errors on $P_s(k)$ into error estimates of model parameters [39]. The Fisher matrix is computed from

$$F_{\alpha\beta} = \frac{V_s}{8\pi^2} \int_{-1}^{1} d\mu \int_{k_{min}}^{k_{max}} k^2 dk \, \frac{\partial \ln P_s(k,\mu)}{\partial p_\alpha} \frac{\partial \ln P_s(k,\mu)}{\partial p_\beta}$$
$$\times \left[\frac{\bar{n}_g P_s(k,\mu)}{\bar{n}_g P_s(k,\mu) + 1} \right]^2, \quad (15)$$

where p_α expresses a set of parameters. One may evaluate some derivative terms analytically:

$$\frac{\partial \ln P_s(k,\mu)}{\partial \delta_\mathcal{R}} = \frac{2}{\delta_\mathcal{R}}, \quad (16)$$

$$\frac{\partial \ln P_s(k,\mu)}{\partial n_s} = \ln \frac{k}{k_0}, \quad (17)$$

$$\frac{\partial \ln P_s(k,\mu)}{\partial \alpha_s} = \frac{1}{2} \left(\ln \frac{k}{k_0} \right)^2. \quad (18)$$

The 1σ error on p_α marginalized over the other parameters is given by $\sigma^2(p_\alpha) = (\boldsymbol{F}^{-1})_{\alpha\alpha}$, where $\boldsymbol{F}^{-1}$ is the inverse of the Fisher matrix. It is sometimes useful to consider projected constraints in a two-parameter subspace to see how two parameters are correlated. We follow the method described around Eq. (37) in [53] for doing this. Another quantity to describe degeneracies between given two parameters, p_μ and p_ν, is the correlation coefficient defined as

$$r(p_\alpha, p_\beta) = \frac{(\boldsymbol{F}^{-1})_{\alpha\beta}}{\sqrt{(\boldsymbol{F}^{-1})_{\alpha\alpha}(\boldsymbol{F}^{-1})_{\beta\beta}}}. \quad (19)$$

If $|r| = 1$, the parameters are totally degenerate, while $r = 0$ means they are uncorrelated.

To calculate $F_{\alpha\beta}$ using Eq. (15), we need to specify k_{min} and k_{max} for a given galaxy survey. We use the upper limit, k_{max}, to exclude information in the non-linear regime, where the linear theory prediction of density fluctuations, Eq. (11), becomes invalid. Following [39], we adopt a conservative estimate for k_{max} by imposing the condition $\sigma_{mass}(R, z) = 0.5$, where $\sigma_{mass}(R, z)$ is the r.m.s. mass fluctuation in a sphere of radius $R = \pi/(2k_{max})$ at a given redshift z. All the Fourier modes below k_{max} are considered as in the linear regime. This idea is partly supported by the simulation-based work in the literature [60–62], while a more careful and quantitative study is needed to understand the impact of non-linearities on cosmological parameter estimates as well as to study how to protect the cosmological information against the systematics. Table I lists k_{max} for each redshift slice of galaxy surveys we shall consider. In addition, we shall show how the results will change with varying k_{max}. As for the minimum wavenumber, we use $k_{min} = 10^{-4}$ Mpc^{-1}, which gives well-converged results for all the cases we consider.

D. Model Parameters

The parameter forecasts derived from the Fisher information formalism depend on the fiducial model and are also sensitive to the choice of free parameters. We include a fairly broad range of the CDM dominated cosmology: the density parameters are $\Omega_m(= 0.27)$, $\Omega_m h^2(= 0.14)$, and $\Omega_b h^2(= 0.024)$ (note that we assume a flat universe); the primordial power spectrum shape parameters are the spectral tilt, $n_s(= 1)$, the running index, $\alpha_s(= 0)$, and the normalization of primordial curvature perturbation, $\delta_\mathcal{R}(= 5.07 \times 10^{-5})$ (the numbers in the parentheses denote the values of the fiducial model). The linear bias parameters, b_1, are calculated for each redshift slice as given in Table I; the fiducial values of the neutrino parameters, f_ν and N_ν^{nr}, are allowed to vary in order to study how the constraints on f_ν and N_ν^{nr} change with the assumed fiducial values. For a survey which consists of N_s redshift slices, we have $8 + N_s$ parameters in total.

As we shall show later, a galaxy survey alone cannot determine all the cosmological parameters simultaneously, but would leave some parameter combinations degenerated. This is especially true when non-relativistic neutrinos are added. Therefore, it is desirable to combine the galaxy survey constraints with the constraints from CMB temperature and polarization anisotropy, in order to lift parameter degeneracies. When computing the Fisher matrix of CMB, we employ 7 parameters: 6 parameters (the parameters above minus the neutrino parameters and the bias parameters) plus the Thomson scattering optical depth to the last scattering surface, $\tau(= 0.16)$. Note that we ignore the effects of non-relativistic neutrinos on the CMB power spectra: their

effects are small and do not add very much to the constraints from the high-z galaxy survey. We then add the CMB Fisher matrix to the galaxy Fisher matrix as $F_{\alpha\beta} = F_{\alpha\beta}^{\mathrm{g}} + F_{\alpha\beta}^{\mathrm{CMB}}$. We entirely ignore the contribution to the CMB from the primordial gravitational waves. We use the publicly-available CMBFAST code [65] to compute the angular power spectrum of temperature anisotropy, C_l^{TT}, E-mode polarization, C_l^{EE}, and their cross correlation, C_l^{TE}. Specifically we consider the noise per pixel and the angular resolution of the Planck experiment that were assumed in [66]. Note that we use the CMB information in the range of multipole $10 \le l \le 2000$.

V. GALAXY SURVEY PARAMETERS

We define the parameters of our hypothetical galaxy surveys so that the parameters resemble the future surveys that are already being planned and seriously pursued. As shown in Eq. (13), the statistical error of the galaxy power spectrum measurement is limited by the survey volume, V_s, as well as the mean number density of galaxies, $\bar{n}_g$. There are two advantages for the high-redshift galaxy surveys. First, given a fixed solid angle, the comoving volume in which we can observe galaxies is larger at higher redshifts than in the local universe. Accordingly, it would be relatively easy to obtain the well-behaved survey geometry, e.g., a cubic geometry that would be helpful to handle the systematics. Second, density fluctuations at smaller spatial scales are still in the linear regime or only in the weakly non-linear regime at higher redshift, which gives us more leverages on measuring the shape of the linear power spectrum.

Of course, we do not always win by going to higher redshifts. Detecting galaxies at higher redshifts is obviously more observationally demanding, as deeper imaging capabilities and better sensitivity for spectrographs are required. To increase the survey efficiency, the use of Multi Object Spectrographs (MOS) or Integral Field Unit (IFU) spectrographs will be favorable. It is therefore unavoidable to have a trade-off in the survey design between the number of spectroscopic targets and the survey volume: for a fixed duration of the survey (or a fixed amount of budget), the total number of spectroscopic targets would be anti-correlated with the survey volume. As carefully discussed in [39], a survey having $\bar{n}_g P_g \gtrsim 3$ over the range of wavenumbers considered is close to an optimal design.

To make the comparison between different survey designs easier, we shall fix the total sky coverage of the surveys to

$$\Omega_{\mathrm{survey}} = 300 \ \mathrm{deg}^2,$$

for all cases. We choose to work with three surveys observing at three different redshift ranges:

- G1: $0.5 < z < 2$

- G2: $2 < z < 4$

- SG: $3.5 < z < 6.5$

where G1 and G2 stands for the "Ground-based galaxy survey" 1 and 2, respectively, while SG stands for the "Space-based Galaxy survey". Table 1 lists detailed survey parameters for each survey design.

A. G1: Ground-based Galaxy Survey at $0.5 < z < 2$

The first survey design, G1, is limited to $0.5 < z < 2$ for the following reasons. One of the reasonable target galaxies from the ground would be giant ellipticals or star-forming galaxies because of their large luminosity. If spectroscopic observations in optical wavebands are available, galaxies having either 3727 Å[OII] emission lines or 4000 Å continuum break may be selected, in which case $z = 1.3$ would be the highest redshift bin, as these spectral line features will move out of the optical wavebands otherwise. If spectroscopy in the near infrared band is available, such as that proposed by the FMOS instrument on Subaru telescope, one may select 6563 Å Hα emission lines which usually have the highest equivalent width among the lines in a star-forming galaxy, in which case a higher redshift, $z \lesssim 2$, may be reached. Based on these considerations, we consider a survey of $0.5 < z < 2$ and subdivide the survey into 3 redshift bins centering at $z = 0.75$, 1.25 and 1.75 with widths $\Delta z = 0.5$. While it is currently difficult to estimate the number density and bias parameters for these galaxies with any certainty because we have a limited knowledge of how such galaxies formed within the CDM hierarchical clustering scenario, we follow the argument given in [39, 40, 42] and assume $\bar{n}_g = 0.5 \times 10^{-3} \ h^3 \ \mathrm{Mpc}^{-3}$. We determine b_1 so that it satisfies the condition $\sigma_{8,g} = 1$ at a given redshift, where

$$\sigma_{8,g} = b_1 \sigma_{8,\mathrm{mass}} \sqrt{1 + \frac{2\beta_m}{3} + \frac{\beta_m^2}{5}}, \qquad (20)$$

with $\beta_m = -d\ln D/d\ln(1+z)$ (i.e. we do not include the massive neutrino contribution when we estimate the fiducial b_1). Note that there is no *a priori* reason to believe that the r.m.s. fluctuation of the number density of galaxies within an $8 \ h^{-1}$ Mpc sphere should be unity; this condition is rather motivated by observations, and it does not have to be true for arbitrary population of galaxies. Nevertheless, this approach seems to provide reasonable values for b_1, and also it makes it easier to compare our results with the previous work that used the same recipe [39, 44]. The values of k_{max} in Table I are computed by $\sigma_{\mathrm{mass}}(R, z) = 0.5$, where $\sigma_{\mathrm{mass}}(R, z)$ is the r.m.s. mass fluctuation in a sphere of radius corresponding to k_{max}, $R = \pi/(2k_{\mathrm{max}})$ (see Sec. IV A).

Survey	z_{center}	$k_{\max}$ $(h\text{Mpc}^{-1})$	Ω_{survey} (deg^2)	V_{s} $(h^{-3}\text{Gpc}^3)$	$\bar{n}_{\text{g}}$ $(10^{-3}\ h^3\text{Mpc}^{-3})$	Bias	$P_g\bar{n}_g$ $(k_{\max})$
G1 $(0.5 < z < 2)$	0.75	0.14	300	0.33	0.5	1.22	4.83
	1.25	0.19	300	0.53	0.5	1.47	2.49
	1.75	0.25	300	0.64	0.5	1.75	1.38
G2 $(2 < z < 4)$	2.25	0.32	300	0.68	0.5	2.03	0.80
	2.75	0.41	300	0.69	0.5	2.32	0.46
	3.25	0.52	300	0.67	0.5	2.62	0.27
	3.75	0.64	300	0.64	0.5	2.92	0.16
SG $(3.5 < z < 6.5)$	4	0.71	300	1.26	5	4	2.19
	5	1.01	300	1.13	5	5	1.04
	6	1.50	300	1.02	5	5.5	0.35

TABLE I: Galaxy survey specifications that we assume in this paper (see Sec. V for the details). We assume a fixed sky coverage (300 deg^2) for all the surveys, and V_{s} and $\bar{n}_{\text{g}}$ are the comoving survey volume and the comoving number density of sampled galaxies for each redshift slice, respectively. z_{center} denotes the center redshift of each redshift slice, and $k_{\max}$ is the maximum wavenumber below which information in the linear power spectrum can be extracted. (We do not use any information above $k_{\max}$ in the Fisher information matrix analysis.) "Bias" denotes the assumed linear bias parameters of sampled galaxies.

B. G2: Ground-based Galaxy Survey at $2 < z < 4$

The second design, G2, probes higher redshifts than G1 by observing different tracers. The primary candidates from the ground in this redshift range would be Lyman-break galaxies or Lyman-α emitters, which are accessible from a deep survey of 8-m class telescopes in optical wavebands. This type of survey has been proposed by the Hobby–Ebery Telescope Dark Energy eXperiment (HET-DEX) [48] and Wide Field Multiple Object Spectrograph (WFMOS) collaborations [47]. To make the comparison easier, we shall assume the same number density as for G1, $0.5 \times 10^{-3}\ h^3$ Mpc^{-3}, for G2. This number corresponds to 4500 galaxies per square degrees, or 1.25 galaxies per square arcminutes for the surface density. We subdivide the redshift range of G2 into 4 bins, 2.25, 2.75, 3.25 and 3.75, and again determine the bias parameters by imposing $\sigma_{8,g}(z) = 1$ at center redshifts of each bin.

C. SG: Space-based Galaxy Survey at $4 < z < 6$

The third design, SG, is a space-based observation which targets galaxies at even higher redshifts, $4 \lesssim z \lesssim 6$. The useful line features will be redshifted into infrared, which makes such high-z galaxies accessible only from space. We determine the survey parameters on the basis of the Cosmic Inflation Probe (CIP) mission [49], one of the nine studies selected by NASA to investigate new ideas for future mission concepts within its Astronomical Search for Origins Program. The CIP is a slitless-grating survey in the near infrared, 2.5–5 μm, which detects Hα emission lines in star-forming galaxies at these redshifts. Being up in space with low background, CIP can achieve a superb sensitivity in infrared. We assume the num-

ber density of $5 \times 10^{-3}\ h^3$ Mpc^{-3} [49], which is larger by one order magnitude than that by the ground based surveys. This number density may be partly justified by the fact that the Lyman break galaxies or the Lyman-α emitters show the similar number density at these redshifts as implied from a deep imaging survey [67], and most of such galaxies are very likely to exhibit an even stronger Hα emission line. For this survey, we assume the bias parameters, $b_1 = 4.5$, 5 and 5.5 for redshift slices of $z = 4$, 5 and 6 with redshift width $\Delta z = 1$, respectively. The bias parameters for this survey have been determined using a different method. We used the mass-weighted mean halo bias above a certain minimum mass, $M_{\min}$. The minimum mass was found such that the number density of dark matter halos above $M_{\min}$ should match the assumed number density of galaxies, $\int_{M_{\min}}^{\infty} dM\ dn/dM = 5 \times 10^{-3}\ h^3$ Mpc^{-3}. Therefore, we basically assumed that each dark matter halo above $M_{\min}$ hosts one Hα emitter on average. One may improve this model by using the Halo Occupation Distribution model, at the expense of increasing the number of free parameters.

Note that we chose these survey designs not to say these are the optimal designs for doing cosmology with high-z surveys, but rather to show how well these planned surveys can constrain the neutrino and inflationary parameters. We are hoping that our results provide some useful information in designing high-z galaxy surveys.

VI. PARAMETER FORECAST: BASIC RESULTS

Tables II and III summarize the basic results of our forecasts for the cosmological parameters from the high-z galaxy redshift surveys combined with the Planck data.

Survey	$f_\nu(m_{\nu,\text{tot}}$ eV$)$	$N_{\nu,\text{fid}}^{\text{nr}}=1$ N_ν^{nr}	$N_{\nu,\text{fid}}^{\text{nr}}=2$ N_ν^{nr}	$N_{\nu,\text{fid}}^{\text{nr}}=3$ N_ν^{nr}	n_s	α_s	Ω_{m}	$\ln\delta_{\mathcal{R}}$	$\ln\Omega_{\text{m}}h^2$	$\ln\Omega_{\text{b}}h^2$
Planck alone	–	–	–	–	0.0062	0.0067	0.035	0.013	0.028	0.011
G1	0.0045(0.059)	0.31	0.64	1.1	0.0038	0.0059	0.0072	0.0099	0.0089	0.0075
G2	0.0033(0.043)	0.20	0.49	0.90	0.0037	0.0057	0.0069	0.0099	0.0086	0.0072
SG	0.0019(0.025)	0.14	0.40	0.80	0.0030	0.0024	0.0041	0.0090	0.0055	0.0050
All (G1+G2+SG)	0.0018(0.024)	0.091	0.31	0.60	0.0026	0.0023	0.0030	0.0089	0.0043	0.0048

TABLE II: The projected 68% error on the cosmological parameters from Planck's CMB data alone (the 1st row) and the high-z galaxy survey data combined with the Planck data (from the 2nd to 5th rows). The quoted error for a given parameter includes marginalization over the other parameter uncertainties. Note that the values with and without parenthesis in the 2nd column are the errors for f_ν and $m_{\nu,\text{tot}}$ (eV), respectively. The fiducial values for the neutrino parameters are $f_{\nu,\text{fid}} = 0.05$ (the neutrino mass fraction; Eq. [1]) and $N_{\nu,\text{fid}}^{\text{nr}} = 3$ (the number of non-relativistic neutrinos), while the fiducial values for the other parameters are given in Sec. IV D. We also vary the fiducial value of $N_{\nu,\text{fid}}^{\text{nr}}$ from 1 to 2 and 3 when quoting the projected errors for N_ν^{nr} with $f_{\nu,\text{fid}} = 0.05$ being fixed, as indicated in the 3rd and 5th columns.

Survey	$f_\nu(m_{\nu,\text{tot}}$ eV$)$	$N_{\nu,\text{fid}}=1$ N_ν^{nr}	$N_{\nu,\text{fid}}=2$ N_ν^{nr}	$N_{\nu,\text{fid}}=3$ N_ν^{nr}	n_s	α_s	Ω_{m}	$\ln\delta_{\mathcal{R}}$	$\ln\Omega_{\text{m}}h^2$	$\ln\Omega_{\text{b}}h^2$
G1	0.0044(0.058)	2.2	7.1	14	0.0037	0.0059	0.0069	0.0099	0.0085	0.0073
G2	0.0033(0.043)	2.1	7.1	13	0.0036	0.0058	0.0059	0.0098	0.0075	0.0066
SG	0.0021(0.028)	1.9	6.4	13	0.0028	0.0021	0.0034	0.0090	0.0048	0.0048
All (G1+G2+SG)	0.0019(0.025)	1.1	3.7	7.4	0.0021	0.0016	0.0017	0.0087	0.0030	0.0045

TABLE III: Same as in the previous table, but for the smaller fiducial neutrino mass fraction, $f_{\nu,\text{fid}} = 0.01$.

Each column shows the projected 1-σ error on a particular parameter, marginalized over the other parameter uncertainties. The 1st row in Table II shows the constraints from the Planck data alone, while the other rows show the constraints from the Planck data combined with each of the high-z galaxy surveys outlined in the previous section. The final row shows the constraints from all the data combined. The difference between these two Tables is the fiducial value for $f_\nu = \Omega_\nu/\Omega_{\text{m}}$: Table II uses $f_\nu = 0.05$, whereas Table III uses a lower value, $f_\nu = 0.01$, as the fiducial value. In addition, in each Table the fiducial value for the number of non-relativistic neutrino species, N_ν^{nr}, is also varied from $N_\nu^{\text{nr}} = 1$ to 2 to 3. Therefore, in Table II the fiducial mass of individual non-relativistic species changes from $m_\nu = 0.66$ to 0.33 to 0.22 eV, whereas in Table III it changes from $m_\nu = 0.13$ to 0.066 to 0.044 eV for $N_\nu^{\text{nr}} = 1$, 2, and 3, respectively. It is also worth showing how the parameter errors are correlated with each other, and we give the parameter correlations in Table VII for the case of SG combined with Planck in Appendix D.

A. Neutrino Parameters

In this paper, we are particularly interested in the capability of future high-z redshift surveys to constraining the neutrino parameters, f_ν and N_ν^{nr}, as well as the shape of the primordial power spectrum, the tilt (n_s) and the running spectral index (α_s). First, we study the neutrino parameters.

The upper panel of Figure 3 shows error ellipses in the subspace of (f_ν, N_ν^{nr}). Two "islands" show two different fiducial models: the left island is (f_ν, N_ν^{nr}) = (0.01, 1), while the right island is (0.05, 3). We find that the errors on f_ν and N_ν^{nr} are only weakly degenerate with each other, implying that the constraints on the two parameters come from different regions of $P(k)$ in k-space, which can be seen more clearly from Figure 2.

1. Total Neutrino Mass

As we have shown in Sec. II, galaxy surveys constrain the total mass of non-relativistic neutrinos by measuring the overall suppression of power at small scales compared with the scales larger than the neutrino free-streaming length, $\Delta P(k)/P(k) \simeq -8f_\nu$ [Eq. (5)]. Tables II and III and Figure 3 (the widths of the error ellipses show the accuracy of constraining the total neutrino mass, $N_\nu^{\text{nr}}m_\nu$) show that the high-z galaxy surveys can provide very tight constraints on the total neutrino mass, $m_{\nu,\text{tot}} = N_\nu^{\text{nr}}m_\nu$, and the constraint improves steadily by going to higher redshifts for a given survey area. The projected error (assuming $f_\nu = 0.05$) improves from $\sigma(m_{\nu,\text{tot}}) = 0.059$ to 0.025 eV for G1 to SG. (The constraint on $m_{\nu,\text{tot}}$ is very similar for $f_\nu = 0.01$.) This is because the suppression rate of the amplitude of the
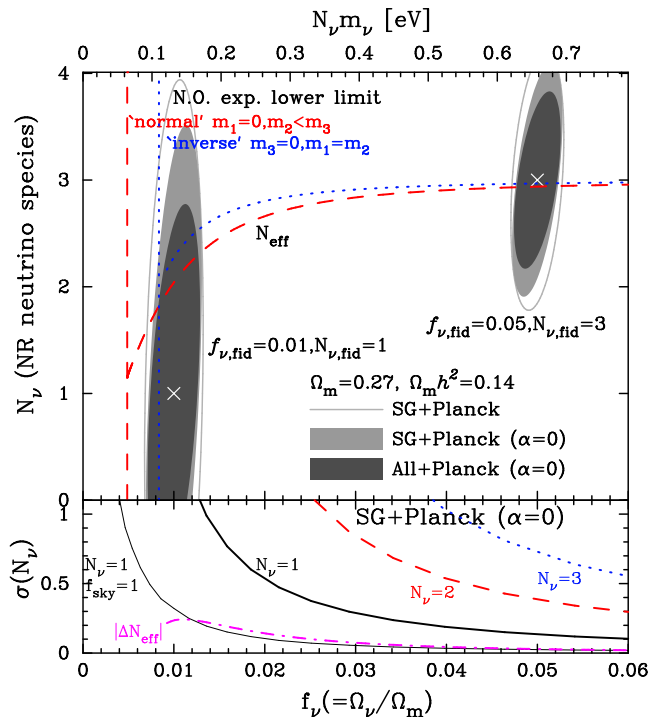
FIG. 4: The projected 68% error on f_ν (upper panel) and N_ν^{nr} (lower panel) against the maximum wavenumber, k_{max}, assuming the information in the linear power spectrum at $k \leq k_{max}$ can be used in the Fisher matrix analysis. The arrows in the above x-axis indicate our nominal k_{max} used in the analysis at each redshift (see Table I). Note that $f_{\nu,fid} = 0.05$ and $N_{\nu,fid}^{nr} = 3$ are assumed.

FIG. 3: *Upper panel*: Projected 68% error ellipses in the neutrino parameter, $(f_\nu$-$N_\nu^{nr})$ plane, expected from the high-z galaxy survey data combined with the Planck data (see Table I for the survey definition). The two fiducial models for f_ν and N_ν^{nr} are considered: the left contours assume $(f_{\nu,fid}, N_{\nu,fid}^{nr}) = (0.01, 1)$, while the right contours assume $(f_{\nu,fid}, N_{\nu,fid}^{nr}) = (0.05, 3)$. The outer thin lines and the middle light-gray contours are the forecasts for SG (the space-based mission at $3.5 < z < 6.5$) plus Planck, without and with a prior on the running spectral index, $\alpha_s = 0$, respectively. The innermost, dark gray contours show the forecasts when all the galaxy surveys (two ground-based surveys and SG) and Planck are combined. The vertical dashed and dotted lines show the lower limits on f_ν implied from the neutrino oscillation experiments assuming the normal and inverted mass hierarchy models, respectively. The dashed and dotted curves then show the effective number of non-relativistic neutrino species, N_{eff}, for the two hierarchy models (see Eq. [21] for the definition). *Lower panel*: The projected 68% on N_ν^{nr} as a function of the fiducial value of f_ν. The thick solid, dashed, and dotted lines use the fiducial values of $N_{\nu,fid}^{nr} = 1, 2$, and 3, respectively. The dot-dashed curve shows the difference between N_{eff} for the normal and inverted mass hierarchy models. The leftmost thin solid line shows the error expected from a hypothetical full-sky SG survey for $N_{\nu,fid}^{nr} = 1$.

linear power spectrum on small scales can be precisely measured by the galaxy survey when combined with the tight constraint on the amplitude of the spectrum on large scales from Planck (also see Table V and Table VII in Appendix D). The steady improvement at higher red-shifts is simply because surveys at higher redshifts can be used to probe smaller spatial scales (i.e., larger k_{max}; see Table I). We find that it is crucial to increase k_{max} as much as possible in order to improve the constraints on the neutrino parameters. Figure 4 shows how one can

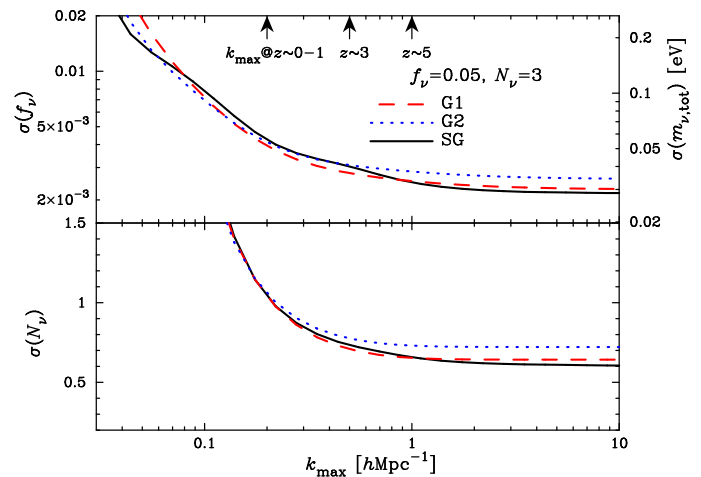reduce the errors on f_ν and N_ν^{nr} by increasing k_{max}.

These results are extremely encouraging. If we *a priori* assume three-flavor neutrinos in compatible with the neutrino oscillation experiments, then it is likely that one can determine the sum of neutrino masses using the high-z galaxy redshift surveys, as the current lower bounds implied from the neutrino oscillation experiments are $m_{\nu,tot} \gtrsim 0.06$ and 0.1 eV for the normal and inverse mass hierarchies, respectively. It should also be noted that a detection of the total mass in the range of $m_{\nu,tot} < 0.1$ eV gives an indirect evidence for the normal mass hierarchy, thereby resolving the mass hierarchy problem.

Our results may be compared with the previous work [31], where $\sigma(m_{\nu,tot}) \approx 0.3$ eV (1σ) was obtained; therefore, our errors are smaller than theirs by a factor of 5–10, even though the survey volume that we assumed is larger only by a factor of 1.5–3 than what they assumed. What drives the improvement? There are two reasons. The first reason is because we consider high-z galaxy surveys, while [31] considered low-z surveys, such as the Sloan Digital Sky Survey, which suffer from much stronger non-linearity. We are therefore using the information on the power spectrum down to larger wavenumbers (i.e., k_{max} is larger). Figure 4 shows that all the galaxy surveys have essentially equal power of constraining the neutrino parameters, when the information up to the same k_{max} is used. However, one cannot do this for low-z surveys because of strong non-linearity. As long as we restrict ourselves to the linear regime, a higher redshift survey is more powerful in terms of constraining the neutrino parameters. Interestingly, the error on the neutrino parameters appears to be saturated at $k_{max} \sim 1$ Mpc^{-1}; thus, the space-based mission, SG, is already nearly optimal for constraining the neutrino parameters for the survey pa-

rameters (especially the number density and bias parameters of sampled galaxies that determine the shot noise contribution to limit the small-scale measurements). The second reason is because our parameter forecast uses the full 2D information in the redshift-space power spectrum (see Eq. (11)) that includes effects of the cosmological distortion and the redshift-space distortion due to peculiar velocity. These effects are very useful in breaking parameter degeneracies. Table V shows that the constraint on $m_{\nu,\mathrm{tot}}$ would be significantly degraded if we did not include the distortion effects. In particular, ignoring the information on the redshift-space distortion, which is consistent with the analysis of [31], leads to a similar-level constraint on $m_{\nu,\mathrm{tot}}$ as theirs. The inclusion of the redshift-space distortion helps break degeneracy between the power spectrum amplitude and the galaxy bias, which in turn helps determine the small-scale suppression due to the neutrino free-streaming.

The projected error on the neutrino total mass might also depend on the fiducial value of $\Omega_{\mathrm{m}}h^2$, as the effect of neutrinos on the power spectrum depends on $f_\nu \propto m_{\nu,\mathrm{tot}}/(\Omega_{\mathrm{m}}h^2)$ [Eq. (1)] [31]. For a given f_ν, a variation in $\Omega_{\mathrm{m}}h^2$ changes $m_{\nu,\mathrm{tot}}$. Now that $\Omega_{\mathrm{m}}h^2$ has been constrained accurately by WMAP, however, we find that our results are not very sensitive to the precise value of $\Omega_{\mathrm{m}}h^2$. We have repeated our analysis for $\Omega_{\mathrm{m}}h^2 = 0.1$, the 2σ-level lower bound from the WMAP results [1], and found very similar results.

2. Number of Non-relativistic Neutrino Species

Galaxy surveys could also be used to determine the *individual* mass of non-relativistic neutrinos, m_ν. As we have shown in Sec. II, galaxy surveys can constrain m_ν by determining the free-streaming scale, $k_{\mathrm{fs}}(z) \propto m_\nu$ [Eq. (2)], from distortion of the shape of the galaxy power spectrum near $k_{\mathrm{fs}}(z)$.

Neutrino oscillation experiments have provided tight limits on the mass square differences between neutrino mass eigenstates as $|m_2^2 - m_1^2| \simeq 7 \times 10^{-5}~\mathrm{eV}^2$ and $|m_3^2 - m_2^2| \simeq 3 \times 10^{-3}~\mathrm{eV}^2$ where m_i denotes mass of the i-th mass eigenstates. We model a family of possible models by the largest neutrino mass, m_ν, motivated by the fact that structure formation is sensitive to most massive species. We may define the effective number of non-relativistic neutrino species as

$$N_{\mathrm{eff}}^{\mathrm{nr}} \equiv 1 + \frac{m_i}{m_\nu} + \frac{m_j}{m_\nu}, \qquad (21)$$

which continuously varies between $1 \leq N_{\mathrm{eff}}^{\mathrm{nr}} \leq 3$. The total neutrino mass is given by $m_{\nu,\mathrm{tot}} = N_{\mathrm{eff}}^{\mathrm{nr}} m_\nu$. We then consider two neutrino mass hierarchy models (we shall assume, by convention, that $m_2 \geq m_1$):

- *Normal mass hierarchy*: $m_\nu = m_3$

  In this model, m_3 is assumed to be the largest mass, and $m_1 < m_2 < m_3$ are allowed. When $m_2, m_1 \ll$ m_3 (the extreme case $m_1 = 0$ eV), $N_{\mathrm{eff}}^{\mathrm{nr}} \simeq 1$. On the other hand, when m_1 and m_2 are comparable to the mass difference between m_2 and m_3, we have $N_{\mathrm{eff}}^{\mathrm{nr}} \simeq 3$ (i.e., three masses are nearly degenerate). Hence, the "normal mass hierarchy" model allows $N_{\mathrm{eff}}^{\mathrm{nr}}$ to vary in the full parameter space, $1 \leq N_{\mathrm{eff}}^{\mathrm{nr}} \leq 3$.

- *Inverted mass hierarchy, $m_1 \sim m_2 = m_\nu$*

  In this model, m_3 is assumed to be the smallest mass, and $m_3 < m_1 < m_2$. A peculiar feature of this model is that N_ν^{nr} cannot be less than 2: when $m_3 = 0$, the possible solutions allowed by the neutrino oscillation experiments are $m_2 \simeq 0.055$ eV and $m_1 \simeq 0.047$ eV or $m_{\nu,\mathrm{tot}} \simeq 0.1$ eV; thus, m_1 and m_2 must be very similar, giving $N_\nu^{\mathrm{nr}} \simeq 2$. Again, when m_3 is comparable to the mass difference between m_2 and m_3, all three masses are degenerate, $N_{\mathrm{eff}}^{\mathrm{nr}} \simeq 3$. Hence, the "inverted mass hierarchy" model allows $N_{\mathrm{eff}}^{\mathrm{nr}}$ to vary only in the limited parameter space, $2 \leq N_{\mathrm{eff}}^{\mathrm{nr}} \leq 3$.

In the upper panel of Figure 3, we show $N_{\mathrm{eff}}^{\mathrm{nr}}$ for the normal mass hierarchy model (dashed line) and for the inverted mass hierarchy model (dotted line). One can see that the two models are indistinguishable (all masses are degenerate) for $f_\nu \gtrsim 0.02$.

How do we constrain N_ν^{nr}? We measure $m_{\nu,\mathrm{tot}}$ from the overall suppression of power at small scales, as described in the previous section. Then we measure m_ν from the "break" of the power spectrum caused by the free-streaming scale, $k_{\mathrm{fs}}(z)$. The number of non-relativistic neutrinos is finally constrained as $N_\nu^{\mathrm{nr}} = m_{\nu,\mathrm{tot}}/m_\nu$, which tells us about the neutrino mass hierarchy. In the 3rd to 5th columns in Table II we show the projected error on N_ν^{nr} from high-z galaxy surveys combined with the Planck data, assuming the fiducial neutrino mass fraction of $f_\nu = 0.05$. As the error depends very much on the fiducial value of N_ν^{nr}, we explore three different fiducial values, $N_{\nu,\mathrm{fid}}^{\mathrm{nr}} = 1$, 2 and 3. As we have described above, however, the first two fiducial values, $N_{\nu,\mathrm{fid}}^{\mathrm{nr}} = 1$ and 2, are inconsistent with the neutrino oscillation experiments if $f_\nu = 0.05$ (all the masses must be nearly degenerate); thus, only the 5th column is actually realistic if there is no sterile neutrino. We find that N_ν^{nr} is going to be difficult to constrain: even when we combine all the high-z galaxy surveys, G1, G2 and SG, the projected error is $\Delta N_\nu^{\mathrm{nr}} = 0.6$. This implies that it is not possible to discriminate between $N_\nu^{\mathrm{nr}} = 2$ and 3 at more than 2-σ, while one can reject $N_\nu^{\mathrm{nr}} = 1$. When the fiducial value of f_ν is small enough to allow for $N_\nu^{\mathrm{nr}} \leq 2$, $f_\nu = 0.01$, the constraints are too weak to be useful (see the 3rd to 5th columns in Table III).

As explained above, if the total neutrino mass is larger than 0.2 eV, $N_{\mathrm{eff}}^{\mathrm{nr}} \simeq 3$ is expected from the neutrino oscillation experiments. The lower panel of Figure 3 shows the projected error on N_ν^{nr} for the SG survey. A model with $N_\nu^{\mathrm{nr}} = 3$ can be detected at more than 1σ level only if $f_\nu \gtrsim 0.04$ ($m_{\nu,\mathrm{tot}} \gtrsim 0.52$ eV). Nevertheless, it should be

	+full Planck (@$k_0 = 0.05$ Mpc^{-1})		@ $k = k_{\text{pivot}}$		
	n_s	α_s	$k_{0,\text{pivot}}$ (Mpc^{-1})	n_s	α_s
Planck alone	0.0062	0.0067	–	–	–
G1	0.0038	0.0059	0.030	0.086	0.035
G2	0.0037	0.0057	0.18	0.018	0.025
SG	0.0030	0.0024	0.48	0.0033	0.0070

TABLE IV: Projected 68% errors on the parameters that characterize the shape of the primordial power spectrum, the tilt (n_s) and the running index (α_s). The left block is the same as the 6th and 7th columns in Table II, which combines the galaxy survey data with the CMB data from Planck, while the right block shows the constraints when the CMB information on n_s and α_s are not used. The left block lists the constraints on n_s and α_s using $k_0 = 0.05$ Mpc^{-1} [see Eq. (C6)] which was chosen such that the Planck data would yield the best constraints. The 1st column in the right block shows the pivot wavenumber at which the errors on n_s and α_s are uncorrelated for a given galaxy survey, and the 2nd and 3rd columns show the constraints on n_s and α_s at the pivot wavenumber, respectively. The space-based galaxy survey at $3.5 < z < 6.5$, SG, on its own yields better constraints on n_s and comparable constraints on α_s compared to Planck alone, when evaluated at its pivot wavenumber. Note that $f_{\nu,\text{fid}} = 0.05$ and $N_{\nu,\text{fid}}^{\text{nr}} = 3$ are assumed.

noted that exploring the constraint on N_ν^{nr} with future surveys is extremely important because any finding of a model with $N_\nu^{\text{nr}} \neq 3$ in this range of f_ν may provide valuable information for the existence of sterile neutrino or new physics. The general trend is that the error on N_ν^{nr} increases as m_ν decreases (i.e., the fiducial value of f_ν decreases or N_ν^{nr} increases). This is because the neutrino free-streaming scale, k_{fs}, is proportional to m_ν: when m_ν is too small, k_{fs} will go out of the k range accessible by galaxy surveys. A possible way to overcome this obstacle is to enlarge the survey volume which, in turn, can lower the minimum wavenumber sampled by the survey. The leftmost curve shows the projected error on N_ν^{nr} for $N_{\nu,\text{fid}}^{\text{nr}} = 1$ from a hypothetical full-sky SG survey at $3.5 < z < 6.5$. We find that such a survey will be able to distinguish between two mass hierarchy models in principle.

FIG. 5: The projected 68% error on n_s (upper panel) and α_s against k_{max}, as in Figure 4.

B. Shape of the Primordial Power Spectrum

The amplitude of the primordial power spectrum appears to be one of the most difficult parameters to measure very accurately. Adding the galaxy survey does not help very much: the constraint on the amplitude improves only by a factor of 1.5 *at most*, even by combining all the data sets. (See the 9th column of Table II and III.) This is because the Planck experiment alone can provide sufficiently tight constraint on the amplitude: Planck allows us to break degeneracy between the amplitude and the optical depth τ by measuring the CMB polarization with high precision (the current accuracy of determining the amplitude, obtained from the WMAP, is about 10%). Adding galaxy surveys does not improve the accuracy of normalization due to the galaxy bias. The constraint on the amplitude could be further improved by adding the weak gravitational lensing data (e.g. see [53, 63, 64]), which directly measures the dark matter distribution. Also, the lensing data are actually sensi-
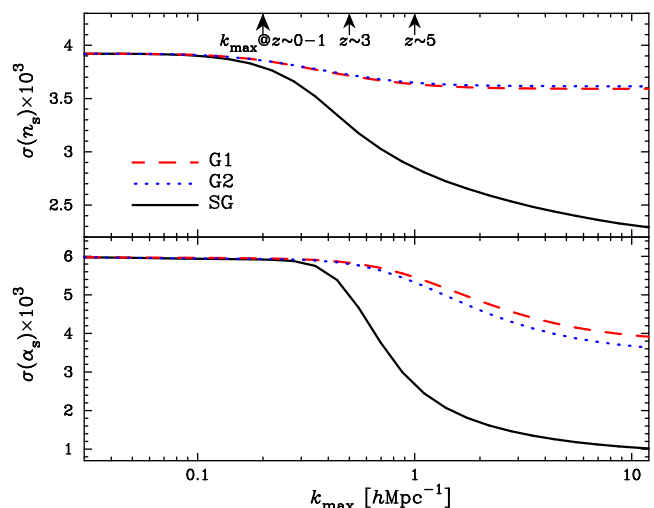
tive to mass clustering in the non-linear regime, and thus would be complementary to the galaxy surveys probing the linear-regime fluctuations.

The interesting parameter is the running spectral index, α_s. Actually G1 or G2 does not improve the constraint on α_s at all: the error shrinks merely by 20%; however, the space-based survey, such as CIP, provides a dramatic improvement over the Planck data, by a factor of nearly 3. This indicates that SG *alone* is at least as powerful as Planck in terms of constraining α_s. (We shall come back to this point below.) The driving force for this improvement is the value of the maximum usable wavenumber for SG, $k_{\text{max}} \sim 1$ Mpc^{-1}, which is substantially greater than that for G1, $k_{\text{max}} \sim 0.2$ Mpc^{-1}, and that for G2, $k_{\text{max}} \sim 0.5$ Mpc^{-1}. Our study therefore indicates that one needs to push k_{max} at least up to $k_{\text{max}} \sim 1$ Mpc^{-1} in order to achieve a significant improvement in the constraint on α_s, for the survey parameters (the number density and bias parameters of sampled
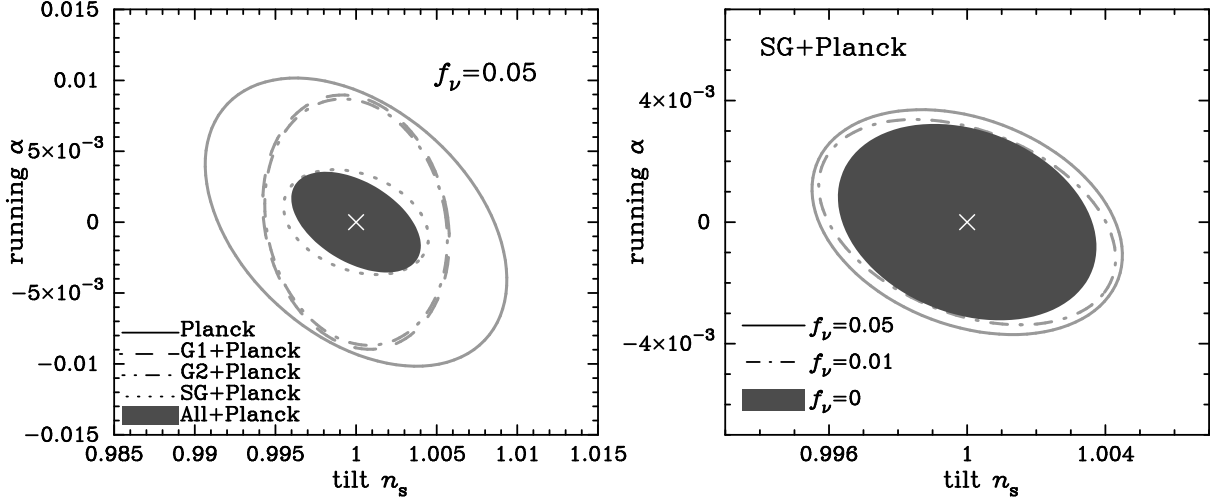
FIG. 6: *Left panel*: Projected 68% error ellipses in the (n_s, α_s) plane from Planck alone (the outermost contour), and the high-z galaxy surveys combined with Planck. The dashed and dot-dashed contours are G1 $(0.5 < z < 2)$ and G2 $(2 < z < 4)$, respectively, while the dotted contour is SG $(3.5 < z < 6.5)$. The highest redshift survey, SG, provides very tight constraints on the shape of the primordial power spectrum. The innermost shaded area shows the constraint from all the galaxy surveys and Planck combined. *Right panel:* Degradation in the constraints on n_s and α_s as a function of the non-relativistic neutrino contribution, f_ν, for SG plus Planck. The effect of non-relativistic neutrinos hardly affects the constraints on n_s and α_s.
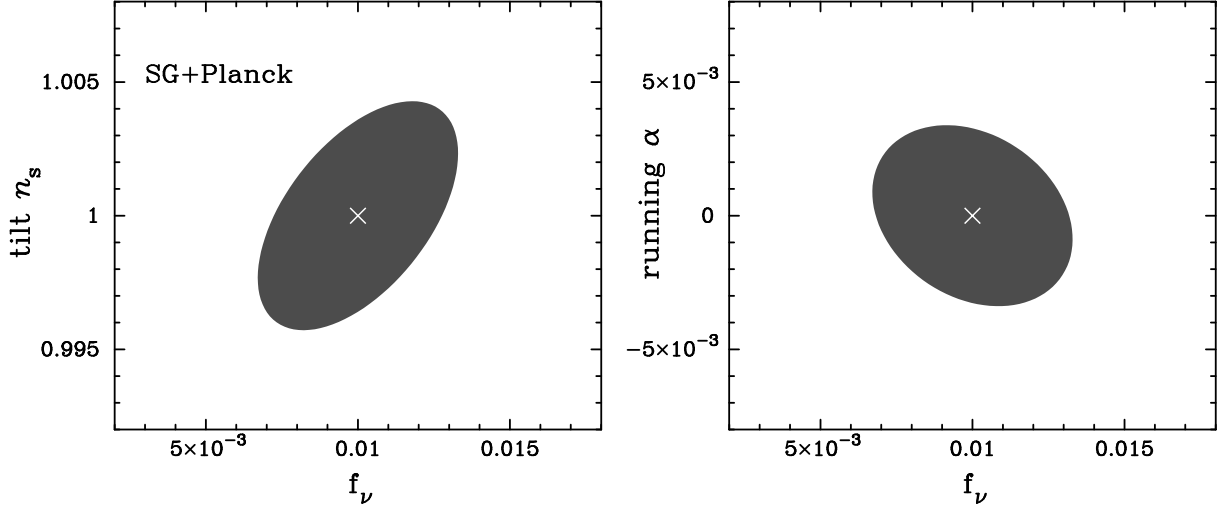

FIG. 7: Projected 68% error ellipses in the (f_ν, n_s) (left panel) and (f_ν, α_s) (right panel) planes, respectively, for SG combined with Planck. Note that the fiducial values of $f_{\nu,\mathrm{fid}} = 0.01$ and $N_{\nu,\mathrm{fid}}^{\mathrm{nr}} = 1$ are assumed.

Survey	No CMB					No Geometric Distortion					No Redshift Space Distortion				
	f_ν	N_ν^{nr}	Ω_{m0}	n_s	α_s	f_ν	N_ν^{nr}	Ω_{m0}	n_s	α_s	f_ν	N_ν^{nr}	Ω_{m0}	n_s	α_s
G1	0.19	11	0.037	0.31	0.22	0.0052	1.0	0.0074	0.0039	0.0059	0.017	3.8	0.0073	0.0039	0.0060
G2	0.082	4.1	0.023	0.10	0.060	0.0043	0.78	0.0073	0.0039	0.0057	0.015	3.0	0.0070	0.0038	0.0058
SG	0.044	2.6	0.0064	0.057	0.013	0.0033	0.64	0.0064	0.0038	0.0025	0.011	2.3	0.0048	0.0032	0.0027

TABLE V: Parameter degradation when some information is thrown away from the analysis. From left to right, CMB, the geometric distortion, or the redshift space distortion has been removed from the analysis. Note that $f_{\nu,\mathrm{fid}} = 0.05$ and $N_{\nu,\mathrm{fid}}^{\mathrm{nr}} = 3$ are assumed.

	V1N5				V5N1				V5N5		
	f_ν	N_ν^{nr}	n_s	α_s	f_ν	N_ν^{nr}	n_s	α_s	f_ν	N_ν^{nr}	n_s	α_s
G1	0.0038	0.83(2.0)	0.0037	0.0059	0.0033	0.59(1.4)	0.0036	0.0057	0.0029	0.50(1.3)	0.0034	0.0057
G2	0.0024	0.71(1.8)	0.0034	0.0052	0.0025	0.59(1.4)	0.0034	0.0051	0.0021	0.46(1.2)	0.0028	0.0040
SG	0.0018	0.66(1.6)	0.0026	0.0018	0.0017	0.49(1.1)	0.0023	0.0018	0.0016	0.42(0.97)	0.0019	0.0013

TABLE VI: Projected 68% errors on the neutrino and power spectrum shape parameters for advanced survey parameters. "V1N5" has a factor of 5 larger number density of galaxies than the fiducial survey, "V5N1" has a factor of 5 larger survey volume, and "V5N5" has a factor of 5 increase in the both quantities. Note that $f_{\nu,\mathrm{fid}} = 0.05$ and $N_{\nu,\mathrm{fid}}^{\mathrm{nr}} = 3$ are assumed, while $f_{\nu,\mathrm{fid}} = 0.01$ and $N_{\nu,\mathrm{fid}}^{\mathrm{nr}} = 1$ are assumed for N_ν^{nr} in the parentheses.

galaxies) we have considered. This can be also clearly found from Figure 5.

On the other hand, the improvement on the tilt, n_s, at $k_0 = 0.05$ Mpc^{-1} is similar for G1, G2, and SG: from a factor of 1.5 to 2. The interpretation of this result is, however, complicated by the fact that the actual constraint depends very much on the value of the pivot scale, k_0, at which n_s is defined. The current value, $k_0 = 0.05$ Mpc^{-1}, was chosen such that the Planck data would provide the best constraint on n_s. On the other hand, as the galaxy survey data probe fluctuations on the smaller spatial scales (larger k), the optimal pivot wavenumber for the galaxy surveys should actually be larger than 0.05 Mpc^{-1}: the optimal pivot wavenumbers for G2 and SG are $k_{0\mathrm{pivot}} = 0.18$ and 0.48 Mpc^{-1}, respectively, where $k_{0\mathrm{pivot}}$ was computed such that the covariance between $n_s(k_{0\mathrm{pivot}})$ and α_s should vanish at $k_{0\mathrm{pivot}}$ and the two parameters would be statistically independent (see [31] for more discussion on this issue; see also [39] for the similar method for constraining the dark energy equation of state at pivot redshift). Table IV lists $k_{0\mathrm{pivot}}$ for G1, G2 and SG, and the errors on $n_s(k_{0\mathrm{pivot}})$ and $\alpha_{s,\mathrm{pivot}}$. Note that we do not use the CMB information on n_s and α_s to derive $k_{0\mathrm{pivot}}$ (but include the CMB information on the other parameters). This Table therefore basically shows how the galaxy survey data alone are sensitive to the shape of the primordial power spectrum. The striking one is SG: the errors on $n_s(k_{0\mathrm{pivot}})$ and α_s are 0.0033 and 0.0070, respectively, which should be compared with those from the Planck data alone, 0.0062 and 0.0067. Therefore, SG alone is at least as powerful as Planck, in terms of constraining the shape of the primordial power spectrum.

The correct interpretation and summary of these results is the following. The Planck data alone cannot constrain the value of n_s very well at small spatial scales (the uncertainty diverges at larger k_0), and the galaxy survey data alone cannot do so at large spatial scales (the uncertainty diverges at smaller k_0). However, when two data sets are combined, *the accuracy in determining n_s becomes nearly uniform at all spatial scales*, and the constraint becomes nearly independent of a particular choice of k_0. This is in fact a huge improvement of the situation, which may not be seen very clearly from just an improvement of n_s defined at a particular k_0. This

is probably best represented by the constraint on α_s we described above: the significant reduction in the uncertainty in α_s for SG indicates that SG in combination with Planck has nearly uniform sensitivity to the shape of the primordial power spectrum from CMB to galaxy scales. This is exactly what one needs for improving constraints on inflationary models.

The left panel of Figure 6 summarizes the constraints on α_s and n_s at $k_0 = 0.05$ Mpc^{-1}. This figure shows the projected error ellipses in the (n_s, α_s) subspace. The overall improvement on the parameter constraint in the 2D sub-space is quite impressive, and it clearly shows the importance of high-z galaxy surveys for improving constraints on the shape of the primordial power spectrum.

Yet, one might be worried about the presence of non-relativistic neutrinos degrading the constraints, α_s in particular, as the neutrinos might mimic the effect of a negative α_s by suppressing the power more at smaller spatial scales. The right panel of Figure 6 basically shows that there is no need to worry: the constraints on n_s and α_s are hardly affected by the non-relativistic neutrinos for $f_\nu = 0 - 0.05$ (the errors on n_s and α_s are degraded less than by $\sim 10\%$). This is because the inflation parameters and the non-relativistic neutrinos change the shape of the galaxy power spectrum in modestly different ways, as explicitly demonstrated in the lower panel of Figure 2, and the high-z galaxy surveys are capable of discriminating these effects. Figure 7 shows the error ellipses in the sub-spaces of (f_ν, n_s) (left panel) and (f_ν, α_s) (right panel). We find that the correlation between n_s and f_ν is modest (the correlation coefficient defined by Eq. (19) is 0.55; see also Table VII), while the correlation between α_s and f_ν is weaker. The most important result from this study is therefore that the 2D joint marginalized constraint on inflationary parameters, n_s and α_s, is hardly affected by the presence of non-relativistic neutrinos.

C. Information from Geometric and Redshift Space Distortion

In Table V we summarize what happens when we throw away some information from our analysis. Without CMB information, the errors on the neutrino parameters inflate significantly by more than an order of magnitude, while

the error on the matter density parameter, Ω_m, is still comparable to or better than that from Planck alone. (Why this is so is explained in the next paragraph.) The errors on n_s and α_s at $k_0 = 0.05$ Mpc^{-1} also inflate.

The geometric distortion effect helps to constrain Ω_m from galaxy surveys alone. The radial distortion constrains the expansion rate, $H(z)$, while the transverse distortion constrains the angular diameter distance, $D_A(z)$. Since $H(z)$ and $D_A(z)$ have different dependences on Ω_m and h for a flat universe, the distortion can determine Ω_m and h simultaneously (Ω_m and $\Omega_m h^2$ for our parameter set). The galaxy surveys at higher redshifts benefit more from the geometric distortion effect.

The redshift space distortion helps to constrain the neutrino parameters, by lifting degeneracy between the neutrino parameters and the galaxy bias. We demonstrate it in the third block of Table V. The errors on the neutrino parameters increase up to nearly a factor of 5 for SG, if we ignore the information from the redshift space distortion. The other parameters are not strongly affected.

D. Variations with Survey Parameters

To guide the survey design, we show how parameter forecasts vary with two key survey parameters, the number density of galaxies and the survey volume. Table VI shows how much one can reduce the projected errors on the key cosmological parameters by increasing the number density of galaxies or the survey volume or both by a factor of 5. These advanced survey parameters are named as

- V1N5: The survey volume is kept the same, while the number density of galaxies is increased by a factor of 5.

- V5N1: The survey volume is increased by a factor of 5, while the number density of galaxies is kept the same.

- V5N5: Both the survey volume and the number density of galaxies are increased by a factor of 5.

Figure 8 shows how the error ellipses for f_ν and N_ν^{nr} will shrink for these advanced parameters.

We find that the most effective way to improve determination of the neutrino parameters, particularly N_ν^{nr}, is to increase the survey volume. One may understand this from Figure 4 — the information on the neutrino parameters saturates at $k_{max} \sim 1$ Mpc^{-1}, and thus there is not much to gain by reducing the power spectrum errors at large k.

On the other hand, one can still improve determination of the parameters that determine the shape of the primordial power spectrum, n_s and α_s, by increasing the number density of galaxies. This is especially true for SG, which probes the largest k_{max}. Therefore, one can
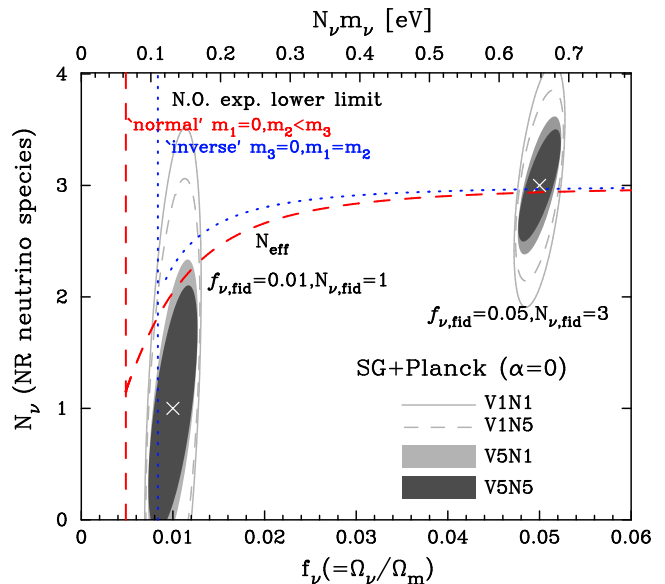

FIG. 8: The same as Figure 3, but for advanced survey parameters for SG combined with Planck, as in Table VI. "V1N1" is the nominal survey parameters given in Table I. Note that zero running, $\alpha_s = 0$, is assumed as a prior, and $f_{\nu,\mathrm{fid}} = 0.05$ and $N_{\nu,\mathrm{fid}}^{nr} = 3$ are assumed.

achieve even better accuracies for constraining inflationary models by either increasing the survey volume or the number density of galaxies, in principle; however, in reality one is eventually going to be limited by our understanding of the galaxy power spectrum in the weakly non-linear regime at large k. In other words, there is not much to gain by reducing the power spectrum errors at large k, if the error is already as small as theoretical uncertainty in the modeling of galaxy power spectrum at the same k. Therefore, increasing the survey volume is probably the best way to improve accuracies of both the neutrino parameters and the inflationary parameters.

VII. CONCLUSIONS AND DISCUSSIONS

The non-relativistic neutrinos and the tilt and running index of the primordial power spectrum cause scale-dependent modifications in the linear power spectrum probed by galaxy redshift surveys. We have shown that one can determine these parameters precisely by fully exploiting the two-dimensional information of galaxy clustering in angular and redshift directions from high-redshift galaxy surveys, when combined with the CMB data from the Planck experiment. The main results are summarized in Tables II and III, and may be graphically viewed in Figures 3 and 6. Our conclusions are two fold.

The first conclusion is for the neutrino parameters. We have found that the future galaxy surveys with $\Omega_s = 300$ deg^2 can provide very tight constraints on the total neutrino mass. The neutrino oscillation experiments have given the solid lower bound on the total neutrino mass,

$m_{\nu,\mathrm{tot}} \gtrsim 0.06$ eV, which is actually larger than the projected error on the total neutrino mass expected from the high-redshift galaxy surveys we have considered, up to by a factor of 2.5 for the space-based survey targeting galaxies at $3.5 < z < 6.5$. If two neutrino species have nearly equal masses (the inverted hierarchy), then the lower bound from the neutrino oscillation experiments, $m_{\nu,\mathrm{tot}} \gtrsim 0.1$ eV, is up to 4 times larger than the projected errors of cosmological experiments. Overall, the high-redshift galaxy surveys combined with Planck allow a positive *detection* of the total neutrino mass rather than the upper limit, improving the constraints on the total neutrino mass by a factor of 20–40 compared with the current cosmological constraints. The error on $m_{\nu,\mathrm{tot}}$ that we have found is smaller than that shown in the previous work (e.g., see [31]) by a factor of 5 – 10, despite the fact that the survey volume we assumed is larger than theirs only by a factor 1.5 – 3. The main reason for the significant improvement is because our analysis exploits the full two-dimensional information in the galaxy power spectrum in redshift space. In particular, the redshift space distortion due to peculiar velocity field significantly helps improve the parameter determinations by breaking degeneracies between the cosmological parameters and the galaxy bias (also see Table V).

In addition, we have carefully investigated how one can use the future surveys to constrain the number of non-relativistic neutrino species, which should play an important role in resolving the neutrino mass hierarchy problem as well as the neutrino absolute mass scale, independently of the total neutrino mass. While we have found that the accuracy needed to discriminate between two models with the same $m_{\nu,\mathrm{tot}}$ but different N_ν^{nr}, $\sigma(N_\nu^{\mathrm{nr}}) \lesssim 1$, is going to be difficult to achieve for the nominal survey designs we considered, one may achieve the desired precision by enlarging the survey volume. It should be stressed here that it is extremely important to exploit independent constraints on $m_{\nu,\mathrm{tot}}$ and N_ν^{nr} from future cosmological observations, as any results unexpected from the point of view of the standard three-flavor neutrino model would imply anomalies in our understanding of the neutrino physics and hints for the new physics. Needless to say, controlling the systematics in such observations is also a crucial issue.

The second conclusion is for the shape of the primordial power spectrum. We have graphically summarized the expected performance of the future galaxy surveys for constraining the tilt, n_s, and the running index, α_s, of the primordial power spectrum in Figure 6. Compared with the constraints from the CMB data alone, the galaxy surveys we have considered can improve the determinations of n_s and α_s by a factor of 2 and 3, yielding $\sigma(n_s) \sim 0.003$ and $\sigma(\alpha_s) \simeq 0.002$, respectively. The high-redshift galaxy surveys allow us to probe galaxy clustering in the linear regime down to smaller length scales than at low redshifts. It is also important to note that the galaxy survey and CMB are sensitive to the primordial power spectrum shape at different k ranges, and

therefore these two probes are nicely complementary to each other in terms of constraining the tilt and the running index at different k. We have explicitly shown that the space-based galaxy survey (SG), such as CIP, has a similar level of precision for constraining n_s and α_s at the pivot scale $k_{0\mathrm{pivot}} \sim 0.5$ Mpc^{-1}, to the Planck experiment at $k_0 = 0.05$ Mpc^{-1} (see Table IV). While it is sometimes argued that simple inflationary models should predict negligible amounts of running index which are out of reach of any experiments, our results show that the projected error on α_s from the SG survey with five times more survey volume is actually as small as α_s predicted by the simple model based on a massive, self-interacting scalar field, $\alpha_s = -(0.8 - 1.2) \times 10^{-3}$. Our results for n_s and α_s are still on the conservative side, as we have ignored the baryonic oscillations in the analysis. We have found that one can reduce the uncertainties in n_s and α_s by a factor of 2–3 by including the baryonic oscillations — however, in that case one might also have to worry about the effect of curvature of the universe and dark energy properties. We report the results of the full analysis elsewhere.

Throughout this paper, we have assumed the standard *three*-flavor neutrinos, some of which have become non-relativistic by the present epoch, as favored by neutrino oscillation experiments and the current theory of particle physics. On the other hand, cosmological observations such as CMB and the large-scale structure can also put independent constraints on the number of *relativistic*, weakly interacting particles just like neutrinos, as a change in the relativistic degrees of freedom directly affects the expansion rate of the universe during the radiation era. For example, an increase in the relativistic degrees of freedom delays the matter-radiation equality, to which the CMB and large-scale structure observables are sensitive. The number of relativistic particles (minus photons) is conventionally expressed in terms of the effective number of neutrino species (i.e., the temperature of additional relativistic species is assumed to be $(4/11)^{1/3}$ of the temperature of photons, just like ordinary neutrinos). The current cosmological bound is $N_\nu = 4.2^{+1.2}_{-1.7}$ (95% C.L.) [68], while the standard model predicts $N_\nu = 3.04$ [70] (also see [69] for the constraint on the abundance and mass of the sterile neutrinos based on the recent cosmological data sets). Hence, it is interesting to explore how one can simultaneously constrain the number of relativistic degrees of freedom before the photon decoupling epoch as well as the number of non-relativistic particle species at low redshifts, N_ν^{nr}, using the future cosmological data sets. Properties of such weakly interacting particles are still difficult to measure experimentally.

It has been shown in the literature that the weak gravitational lensing [53, 72, 73] or the number count of galaxy clusters [74, 75] can also be a powerful probe of the cosmological parameters. Different methods are sensitive to the structure formation at different ranges of redshifts and wavenumbers, and have different dependence on the

cosmological parameters. More importantly, they are subject to very different systematics. Hence, by combining several methods including the galaxy surveys considered in this paper, one can check for systematics inherent in one particular method. The combination of different methods may also reduce statistical errors on the cosmological parameters. While it is worth exploring this issue carefully, we can easily imagine that, for the neutrino parameters, the weak lensing or the cluster number count does not improve $N_\nu^{\rm nr}$ very much. To constrain $N_\nu^{\rm nr}$ better one has to find a way to probe very large spatial scales, larger than the neutrino free-streaming scales; however, these methods probe only very small spatial scales where fluctuations have already become non-linear. (They may provide improvements in the determination of $m_{\nu,\rm tot}$.)

There is a promising way to check for systematics and improve the parameter determinations using the galaxy survey alone. While we have been assuming that perturbations are strictly linear and hence perfectly Gaussian, in reality small non-linearity always exists. The corrections to the power spectrum due to such small non-linearity may be calculated analytically using the higher-order cosmological perturbation theory (see [76] for a review), which works extremely well at $z > 2$ (Komatsu and Jeong, in preparation). Using the same higher-order cosmological perturbation theory, one may also compute the higher-order statistics, such as the bispectrum, which is a very powerful tool to check for systematics due to non-linearity in matter clustering, redshift space distortion, and galaxy bias [77, 78]. Also, the bispectrum and power spectrum have different cosmological dependences [53, 79]; thus, it is naturally expected that combining the two would improve the determinations of cosmological parameters. The results of our investigation along these lines will be reported elsewhere.

No matter how powerful the bispectrum could be in terms of checking for systematics, better models for non-linearity in redshift-space distortion and galaxy bias are definitely required for our projected errors to be actually realized. A good news is that we do not need a fully non-linear description of either component: we always restrict ourselves to the "weakly non-linear regime" where perturbation theory should still be valid. Having an accurate model for the redshift space distortion in the weakly non-linear regime is important for the precise determination of the total neutrino mass, as the redshift distortion plays a major role in lifting the degeneracy between the galaxy bias and the matter power spectrum amplitude (see Table V what happens when the redshift space distortion is ignored). Recently, a sophisticated model of the distortion effect including the weak non-linear correction was developed in [71] based on the analytic method as well as the simulations. Likewise, it will be quite possible to develop a sufficiently accurate, well-calibrated model of the distortion effect at least on large length scales, based on adequate simulations. While we have employed a scale-independent linear bias throughout this paper, this model must break down even at weakly non-linear

regime. Analytical [80] as well as numerical [61, 62, 81] work has shown that deviations from a scale-independent bias do exist even on large spatial scales. This effect would also become particularly important for the precision measurements of the baryonic oscillations for constraining properties of dark energy. Therefore, careful and systematic investigations based on both analytical and numerical tools are needed to understand the realistic effect of scale-dependent bias on estimates of the cosmological parameters. As we have mentioned already, information from the higher-order statistics in the galaxy clustering would be a powerful diagnosis tool to check for systematics due to non-linear bias. As perturbation theory predicts that the galaxy power spectrum and bispectrum should depend on the galaxy bias differently, one can directly determine the galaxy bias and cosmological parameters simultaneously, by combining the two statistical quantities [77–79, 82, 83]. This method should also allow us to see a potential scale-dependent biasing effect from the epoch of reionization [84].

Finally, let us comment on survey parameters. In order to make our discussion general, we have considered three hypothetical surveys which are different in their redshift coverage and the number density of targeted galaxies (see Sec. V for the survey definition). We have also explored how the parameter errors would change when the survey parameters are varied from the fiducial values (see Table VI and Figure 8). Increasing a survey volume has a greater impact on the parameter errors compared with increasing the numbers of targeted galaxies for a given survey volume. We are hoping that our results provide useful information to help to define an optimal survey design to attain the desired accuracy on the parameter determinations, given the limited observational resources and budget.

APPENDIX A: PROPERTIES OF COSMOLOGICAL NEUTRINOS

1. Mass Density

The present-day mass density of non-relativistic neutrinos is given by

$$\rho_\nu^{\rm nr} = \sum_{i=1}^{N_\nu^{\rm nr}} m_{\nu,i} n_{\nu,i}, \tag{A1}$$

where i runs over the neutrino species *that are non-relativistic*, and $N_\nu^{\rm nr}$ is the number of non-relativistic neutrino species. We assume that some of the standard three active neutrinos are massive and thus $0 \leq N_\nu^{\rm nr} \leq 3$. These neutrinos were in thermal equilibrium with other particles at early times until they decoupled from the primordial plasma slightly before electron-positron annihilation. Since they were still relativistic when they decoupled, their distribution function after decoupling is still given by that of a massless Fermion. After electron-positron annihilation, the temperature of photons became higher than the temperature of neutrinos by a factor of $(11/4)^{1/3}$. Thus, the neutrino number density of each species, n_ν, at a redshift relevant for a galaxy survey is given by the relativistic formula:

$$\begin{aligned} n_\nu &= \frac{3\zeta(3)}{2\pi^2} T_\nu^3 \\ &\simeq 112(1+z)^3 \ {\rm cm}^{-3}, \end{aligned} \tag{A2}$$

where $\zeta(3) \simeq 1.202$ and $T_\nu = (4/11)^{1/3} T_{\gamma 0}(1+z)$, where $T_{\gamma 0}$ is the present-day photon temperature and we have assumed $T_{\gamma 0} = 2.725$ K [50]. Note that the number density includes the contribution from anti-neutrinos as well, and does not depend on neutrino species, $n_\nu = n_{\nu,i}$. The density parameter of non-relativistic neutrinos is thus given by

$$\begin{aligned} \Omega_\nu &\equiv \frac{8\pi G \rho_\nu^{\rm nr}}{3H_0^2} = \frac{8\pi G n_\nu}{3H_0^2} \sum_{i=1}^{N_\nu^{\rm nr}} m_{\nu,i} \\ &\simeq \frac{\sum_i m_{\nu,i}}{94.1 h^2 \ {\rm eV}}. \end{aligned} \tag{A3}$$

Since $\Omega_\nu h^2$ must be less than the density parameter of dark matter, $\Omega_{\rm cdm} h^2 \simeq 0.112$, the total mass of non-relativistic neutrinos must satisfy the following cosmological bound,

$$\sum_{i=1}^{N_\nu^{\rm nr}} m_{\nu,i} \lesssim 10.5 \ {\rm eV}. \tag{A4}$$

2. Non-relativistic Epoch

Neutrinos became non-relativistic when the mean energy per particle given by

$$\langle E \rangle = \frac{7\pi^4}{180\zeta(3)} T_\nu \simeq 3.15 T_\nu, \tag{A5}$$

fell below the mass energy, $m_{\nu,i}$. The temperature at which a given neutrino species became non-relativistic, $T_{\nu,i}^{\rm nr}$, is thus given by

$$T_{\nu,i}^{\rm nr} \equiv \frac{180\zeta(3)}{7\pi^4} m_{\nu,i} \simeq 3680 \left(\frac{m_{\nu,i}}{1 \ {\rm eV}}\right) \ {\rm K}. \tag{A6}$$

The redshift at which a given neutrino species became non-relativistic is

$$1 + z_{{\rm nr},i} \simeq 1890 \left(\frac{m_{\nu,i}}{1 \ {\rm eV}}\right). \tag{A7}$$

As the current constraints from the galaxy power spectrum at $z \sim 0$ already suggest $m_{\nu,i} \lesssim 1$ eV, it is certain that neutrinos became non-relativistic during the matter-dominated era. The comoving wavenumber corresponding to the Hubble horizon size at $z_{\rm nr}$ is thus given by

$$\begin{aligned} k_{{\rm nr},i} &\equiv \frac{H(z_{{\rm nr},i})}{1 + z_{{\rm nr},i}} = \frac{\Omega_m^{1/2} h (1 + z_{{\rm nr},i})^{1/2}}{2998 \ {\rm Mpc}} \\ &\simeq 0.0145 \left(\frac{m_{\nu,i}}{1 \ {\rm eV}}\right)^{1/2} \Omega_m^{1/2} h \ {\rm Mpc}^{-1}. \end{aligned} \tag{A8}$$

Note that this value is smaller than that given in [31] by a factor of $\simeq \sqrt{3.15}$. They assumed that neutrinos became non-relativistic when $T_\nu = m_\nu$, rather than $T_\nu = (180\zeta(3)/7\pi^2) m_\nu \simeq m_\nu/3.15$.

3. Neutrino Free-streaming Scale

Density perturbations of non-relativistic neutrinos grow only when the comoving wavenumber of perturbations is below the free-streaming scale, $k_{\rm fs}$, given by

$$k_{{\rm fs},i}(z) \equiv \sqrt{\frac{3}{2}} \frac{H(z)}{(1+z)\sigma_{v,i}(z)}, \tag{A9}$$

where $\sigma_{v,i}^2(z)$ is the velocity dispersion of neutrinos and given in [25] as

$$\begin{aligned} \sigma_{v,i}^2(z) &\equiv \frac{\int \frac{d^3p \ p^2/m^2}{\exp[p/T_\nu(z)]+1}}{\int \frac{d^3p}{\exp[p/T_\nu(z)]+1}} = \frac{15\zeta(5)}{\zeta(3)} \frac{T_\nu^2(z)}{m_{\nu,i}^2} \\ &= \frac{15\zeta(5)}{\zeta(3)} \left(\frac{4}{11}\right)^{2/3} \frac{T_\gamma^2(0)(1+z)^2}{m_{\nu,i}^2}, \end{aligned} \tag{A10}$$

where $\zeta(5) \simeq 1.037$. Hence,

$$k_{{\rm fs},i}(z) \simeq \frac{0.677}{(1+z)^{1/2}} \left(\frac{m_{\nu,i}}{1 \ {\rm eV}}\right) \Omega_m^{1/2} h \ {\rm Mpc}^{-1}. \tag{A11}$$

Neutrino density perturbations with $k > k_{\text{fs},i}$ cannot grow because pressure gradient prevents neutrinos from collapsing gravitationally; thus, neutrinos are effectively smooth at $k > k_{\text{fs},i}$, and the power spectrum of neutrino perturbations is exponentially suppressed. Note that Eq. (A9) is exactly the same as the Jeans scale in an expanding universe for collisional particles, if σ_v is replaced by the speed of sound.

APPENDIX B: INFLATIONARY PREDICTIONS

1. Generic Results

Inflationary predictions are commonly expressed in terms of the shape of the primordial power spectrum of curvature perturbations in comoving gauge, $\mathcal{R}$:

$$\langle \mathcal{R}_{\mathbf{k}} \mathcal{R}_{\mathbf{k}'}^* \rangle = (2\pi)^3 P_{\mathcal{R}}(k) \delta^{(3)}(\mathbf{k} - \mathbf{k}'), \qquad \text{(B1)}$$

where

$$\frac{k^3 P_{\mathcal{R}}(k)}{2\pi^2} = \delta_{\mathcal{R}}^2 \left(\frac{k}{k_0} \right)^{-1 + n_s + \frac{1}{2}\alpha_s \ln(k/k_0)}. \qquad \text{(B2)}$$

Here, n_s and α_s are called the "tilt" and "running index" of the primordial power spectrum. These parameters are related to the shape of potential, $V(\phi)$, of an *inflaton* field, ϕ, a field which caused inflation, as [8]

$$n_s - 1 = M_{\text{pl}}^2 \left[-3 \left(\frac{V'}{V} \right)^2 + 2 \left(\frac{V''}{V} \right) \right], \qquad \text{(B3)}$$

$$\begin{aligned} \alpha_s = 2 M_{\text{pl}}^4 \Bigg[& 4 \left(\frac{V'}{V} \right)^2 \left(\frac{V''}{V} \right) - 3 \left(\frac{V'}{V} \right)^4 \\ & - \left(\frac{V'V'''}{V^2} \right) \Bigg], \end{aligned} \qquad \text{(B4)}$$

where primes denote derivatives with respect to ϕ, and $M_{\text{pl}} \equiv (8\pi G)^{-1/2} = 2.4 \times 10^{18}$ GeV is the reduced Planck mass. Successful inflationary models must yield sufficiently large number of e-folds for the expansion of the universe, N, before inflation ends at t_{end} when ϕ rolls down on the potential to $\phi = \phi_{\text{end}}$:

$$N = \int_t^{t_{\text{end}}} dt\, H(t) \approx \frac{1}{M_{\text{pl}}^2} \int_{\phi_{\text{end}}}^{\phi} d\phi \frac{V}{V'}, \qquad \text{(B5)}$$

which has to be at least as large as 50. This condition requires $|n_s - 1|$ and $|\alpha_s|$ to be much less than unity, while exact values depend on specific inflationary models (i.e., the shape of $V(\phi)$). Therefore, precision determination of n_s and α_s is a very powerful tool for constraining inflationary models.

2. Specific Examples

An illustrative example of inflationary models is inflation caused by a massive, self-interacting real scalar field:

$$V(\phi) = \frac{1}{2} m_\phi^2 \phi^2 + \frac{1}{4} \lambda \phi^4, \qquad \text{(B6)}$$

where m_ϕ is the mass of ϕ and λ (> 0) is the coupling constant of self-interaction. The mass term and the interaction term equal when $\phi = \phi_c$, where

$$\phi_c \equiv m_\phi \sqrt{\frac{2}{\lambda}}. \qquad \text{(B7)}$$

The mass term dominates when $\phi < \phi_c$, while the interaction term dominates when $\phi > \phi_c$. One obtains

$$N \approx \frac{\phi^2}{8M_{\text{pl}}^2} + \frac{\phi_c^2}{16M_{\text{pl}}^2} \ln \left(1 + 2\frac{\phi^2}{\phi_c^2} \right), \qquad \text{(B8)}$$

$$\begin{aligned} n_s - 1 = & -\frac{8M_{\text{pl}}^2}{\phi^2} \\ & \times \frac{1 + \frac{5}{2}\frac{\phi^2}{\phi_c^2} + 3\frac{\phi^4}{\phi_c^4}}{\left(1 + \frac{\phi^2}{\phi_c^2} \right)^2}, \end{aligned} \qquad \text{(B9)}$$

$$\begin{aligned} \alpha_s = & -\frac{32M_{\text{pl}}^4}{\phi^4} \\ & \times \frac{\left(1 + 2\frac{\phi^2}{\phi_c^2} \right) \left(1 + 3\frac{\phi^2}{\phi_c^2} + 2\frac{\phi^4}{\phi_c^4} + 3\frac{\phi^6}{\phi_c^6} \right)}{\left(1 + \frac{\phi^2}{\phi_c^2} \right)^4} \end{aligned} \qquad \text{(B10)}$$

Let us take the limit of mass-term driven inflation, $\phi \ll \phi_c$. One finds

$$N \rightarrow \frac{\phi^2}{4M_{\text{pl}}^2}, \qquad \text{(B11)}$$

$$n_s - 1 \rightarrow -\frac{8M_{\text{pl}}^2}{\phi^2} = -\frac{2}{N}, \qquad \text{(B12)}$$

$$\alpha_s \rightarrow -\frac{32M_{\text{pl}}^4}{\phi^4} = -\frac{2}{N^2}. \qquad \text{(B13)}$$

For $N = 50$, $n_s = 0.96$ and $\alpha_s = -0.8 \times 10^{-3}$. In the opposite limit, self-coupling driven inflation, $\phi \gg \phi_c$, one finds

$$N \rightarrow \frac{\phi^2}{8M_{\text{pl}}^2}, \qquad \text{(B14)}$$

$$n_s - 1 \rightarrow -\frac{24M_{\text{pl}}^2}{\phi^2} = -\frac{3}{N}, \qquad \text{(B15)}$$

$$\alpha_s \rightarrow -\frac{192M_{\text{pl}}^4}{\phi^4} = -\frac{3}{N^2}. \qquad \text{(B16)}$$

For $N = 50$, $n_s = 0.94$ and $\alpha_s = -1.2 \times 10^{-3}$. These simple examples show that a precision of $\sigma(n_s) \sim 10^{-3}$ is sufficient for discriminating between models, while $\sigma(\alpha_s) \sim 10^{-3}$ may allow us to detect α_s from simple (though not the simplest) inflationary models driven by a massive scalar field with self-coupling.

APPENDIX C: NORMALIZING POWER SPECTRUM

While inflation predicts the power spectrum of $\mathcal{R}$, what we observe from galaxy redshift surveys is the power spectrum of matter density fluctuations, δ_m. In this section we derive the conversion from $\mathcal{R}$ during inflation to δ_m at a particular redshift after the matter-radiation equality.

Let us begin by writing the Poisson equation in Fourier space,

$$-k^2\Psi_{\mathbf{k}}(a) = 4\pi G\rho_m(a)\delta_{m,\mathbf{k}}(a)a^2 = \frac{3H_0^2\Omega_{\mathrm{m}}}{2}\frac{\delta_{m,\mathbf{k}}(a)}{a}. \tag{C1}$$

where Ψ is gravitational potential in the usual (Newtonian) sense $(g_{00} = -1 + 2\Psi)$. Cosmological perturbation theory relates Ψ after the matter-radiation equality to $\mathcal{R}$ during inflation as

$$\Psi_{\mathbf{k}}(a) = -\frac{3}{5}\mathcal{R}_{\mathbf{k}}T(k)\frac{D_{cb\nu}(k,a)}{a}, \tag{C2}$$

where $D_{cb\nu}(k,a)$ is the linear growth factor of total matter perturbations including CDM, baryons and non-relativistic neutrinos, and $T(k)$ is the linear transfer function. Note that the transfer function and the growth rate are normalized such that $T(k) \to 1$ as $k \to 0$ and $D_{cb\nu}/a \to 1$ as $k \to 0$ during the matter era. (We assume that neutrinos became non-relativistic during the matter-dominated era.) Hence,

$$\delta_{m,\mathbf{k}}(a) = \frac{2k^2}{5H_0^2\Omega_{\mathrm{m}}}\mathcal{R}_{\mathbf{k}}T(k)D_{cb\nu}(k,a), \tag{C3}$$

which gives the power spectrum of δ_m,

$$P(k,a) = \left(\frac{2k^2}{5H_0^2\Omega_{\mathrm{m}}}\right)^2 P_{\mathcal{R}}(k)T^2(k)D_{cb\nu}^2(k,a), \tag{C4}$$

after the matter-radiation equality. The WMAP collaboration has determined the normalization of $k^3P_{\mathcal{R}}(k)/(2\pi^2)$ at $k = k_0 = 0.05$ Mpc^{-1} as

$$\delta_{\mathcal{R}}^2 = 2.95 \times 10^{-9}A, \tag{C5}$$

where A is a constant of order unity (Eq. [32] of [85]). Putting these results together, we finally obtain the power spectrum of density perturbations normalized to WMAP:

$$\frac{k^3P(k,z)}{2\pi^2} = 2.95 \times 10^{-9}A\left(\frac{2k^2}{5H_0^2\Omega_{\mathrm{m}}}\right)^2$$
$$\times D_{cb\nu}^2(k,z)T^2(k)\left(\frac{k}{k_0}\right)^{-1+n_s+\frac{1}{2}\alpha_s\ln(k/k_0)} \tag{C6}$$

APPENDIX D: CORRELATIONS BETWEEN PARAMETER ESTIMATES

It is worth noting how the parameter estimations are correlated with each other for a given survey, which can be quantified by the correlation coefficients defined by Eq. (19). Table VII gives the correlation matrix for the parameters for SG combined with Planck.

[1] C. Bennet et al., Astrophys. J. Suppl. **148**, 1 (2003).
[2] M. Tegmark et al., Phys. Rev. D **69**, 103501 (2004).
[3] U. Seljak et al., Phys. Rev. D **71**, 103515 (2005).
[4] M. Jarvis, B. Jain, G. Bernstein and D. Dolney, astro-ph/0502243.
[5] P. J. E. Peebles and J. T. Yu, Astrophys. J. **162**, 815 (1970).
[6] R. A. Sunyaev and Ya. B. Zel'dovich, Astrophys. Sp. Sci. **7**, 3 (1970).
[7] J. R. Bond and G. Efstathiou, Astrophys. J. Lett. **285**, 45 (1984).
[8] A. R. Liddle and D. H. Lyth, *Cosmological Inflation and the Large-Scale Structure*, Cambridge University Press (2000).
[9] S. Dodelson, *Modern Cosmology* Academic Press, San Diego, (2003).
[10] G. Hinshaw et al., Astrophys. J. Suppl. **148**, 135 (2003).
[11] A. Kogut et al., Astrophys. J. Suppl. **148**, 161 (2003).
[12] D. J. Eisenstein et al., Astrophys. J. **633**, 560 (2005).
[13] S. Cole, Mon. Not. Roy. Astr. Soc. **362**, 505 (2005).
[14] A. G. Riess et al., Astron. J. **116**, 1009 (1998).
[15] S. Perlmutter et al., Astrophys. J. **517**, 565 (1999).
[16] P. J. E. Peebles and B. Ratra, Rev. Mod. Phys. **75**, 559 (2003).
[17] N. Bartolo, E. Komatsu, S. Matarrese and A. Riotto, Phys. Rept. **402**, 103 (2004).
[18] W. J. Percival et al., Mon. Not. Roy. Astr. Soc. **327**, 1297 (2001).
[19] H. V. Peiris, et al., Astrophys. J. Suppl. **146**, 213 (2003).
[20] S. Fukuda et al. [Super-Kamiokande Collaboration], Phys. Rev. Lett. **85**, 3999 (2000).
[21] S. N. Ahmed et al. [SNO Collaboration], Phys. Rev. Lett. **92**, 181301 (2004).
[22] K. Eguchi et al. [KamLAND Collaboration], Phys. Rev. Lett. **90**, 021802 (2003).
[23] T. Arakki et al. [KamLAND Collaboration], Phys. Rev. Lett. **94** 081801 (2005).
[24] R. D. McKeown and P. Vogel, Phys. Rep. **394**, 315 (2004).
[25] J. R. Bond, G. Efstathiou and J. Silk, Phys. Rev. Lett. **45**, 1980 (1980).
[26] J. R. Bond and A. Szalay, Astrophys. J. **276**, 443 (1983).
[27] D. Pogosyan and A. Starobinsky, Mon. Not. Roy. Astr. Soc. **265**, 507 (1993)
[28] D. Pogosyan and A. Starobinsky, Astrophys. J. **447**, 465 (1995)

	Ω_m	$\delta_\mathcal{R}$	f_ν	N_ν^nr	n_s	α_s	$\Omega_\mathrm{m}h^2$	$\Omega_\mathrm{b}h^2$	τ	$b_1(z=4)$	$b_1(z=5)$	$b_1(z=6)$
Ω_m	1	0.079	-0.28	-0.79	-0.68	-0.32	0.94	-0.41	-0.073	-0.96	-0.96	-0.96
$\delta_\mathcal{R}$	0.079	1	0.81	0.24	0.10	-0.17	0.090	-0.001	0.98	-0.14	-0.16	-0.17
f_ν	-0.28	0.81	1	0.39	0.55	-0.26	-0.27	0.033	0.86	0.30	0.28	0.27
N_ν^nr	-0.79	0.24	0.39	1	0.30	0.45	-0.70	0.43	0.34	0.79	0.78	0.78
n_s	-0.68	0.10	0.55	0.30	1	-0.29	-0.64	0.25	0.24	0.64	0.64	0.63
α_s	-0.32	-0.17	-0.26	0.45	-0.29	1	-0.29	0.17	-0.13	0.35	0.35	0.35
$\Omega_\mathrm{m}h^2$	0.94	0.090	-0.27	-0.70	-0.64	-0.29	1	-0.10	-0.073	-0.90	-0.90	-0.90
$\Omega_\mathrm{b}h^2$	-0.41	-0.001	0.033	0.43	0.25	0.17	-0.10	1	0.022	0.40	0.40	0.40
τ	-0.073	0.98	0.86	0.34	0.24	-0.13	-0.073	0.022	1	0.0071	-0.0086	-0.021
$b_1(z=4)$	-0.96	-0.14	0.30	0.79	0.64	0.35	-0.90	0.40	0.0071	1	0.99	0.99
$b_1(z=5)$	-0.96	-0.16	0.28	0.78	0.64	0.35	-0.90	0.40	-0.0086	0.99	1	0.99
$b_1(z=6)$	-0.96	-0.17	0.27	0.78	0.63	0.35	-0.90	0.40	-0.021	0.99	0.99	1

TABLE VII: The correlation matrix for parameter estimation errors for SG combined with Planck.

[29] C.-P. Ma and E. Bertschinger, Astrophys. J. **455**, 7 (1995).
[30] C.-P. Ma, Astrophys. J. **471**, 13 (1996).
[31] W. Hu, D. Eisensttein and M. Tegmark, Phys. Rev. Lett. **80**, 5255 (1998).
[32] S. Hannestad, Phys. Rev. D **67**, 085017 (2003).
[33] Ø. Elgarøy and O. Lahav, New.J.Phys. **7**, 61 (2005).
[34] O. Lahav and Y. Suto, Living Reviews in Relativity **7**, 1 (2004).
[35] S. Hannestad, astro-ph/0511595.
[36] D. N. Spergel et al., Astrophys. J. Suppl. **148**, 175 (2003).
[37] J. Bonn et al., Nucl.Phys.B (Proc. Suppl.) **91**, 273 (2001).
[38] A. Aguilar et al. [LSND Collaboration], Phys. Rev. D **64**, 112007 (2001).
[39] H.-J. Seo and D. Eisenstein, Astrophys. J. **598**, 720 (2003).
[40] T. Matsubara and A. Szalay, Phys. Rev. Lett. **90**, 021302 (2003)
[41] W. Hu and Z. Haiman, Phys. Rev. D **68**, 063004 (2003).
[42] C. Blake and K. Glazebrook, Astrophys. J. **594**, 665 (2003).
[43] K. Glazebrook and C. Blake, Astrophys. J. in press (astro-ph/0505608).
[44] T. Matsubara, Astrophys. J. **615**, 573 (2004).
[45] K. Yamamoto, B. A. Bassett and H. Nishioka, Phys. Rev. Lett. **94**, 051301 (2005).
[46] M. Kimura et al., Proceedings of the SPIE, **4841**, 974 (2003)
[47] K. Glazebrook et al., astro-ph/0507457.
[48] G. J. Hill, K. Gebhardt, E. Komatsu and P. J. MacQueen, AIP Conf. Proc., **743**, 224 (2004).
[49] G. J. Melnick et al., The NASA Origins Probe Mission Study Report, "*The Cosmic Inflation Probe: Study Report*" (2005). See also http://cfa-www.harvard.edu/cip.
[50] J. C. Mather et al., Astrophys. J. **512**, 511 (1999).
[51] W. Hu and D. Eisensttein, Astrophys. J. **498**, 497 (1998).
[52] W. Hu and D. Eisenstein, Astrophys. J. **511**, 5 (1999).
[53] M. Takada and B. Jain, Mon. Not. Roy. Astr. Soc. **348**, 897 (2004).
[54] C. Alcock and B. Paczynski, Nature (London) , **281** 358

(1979).
[55] T. Matsubara and Y. Suto, Astrophys. J. Lett., **470**, 1 (1996).
[56] W. E. Ballinger, J. A. Peacock and A. F. Heavens, Mon. Not. Roy. Astr. Soc., **282**, 877 (1996).
[57] N. Kaiser, Mon. Not. Roy. Astr. Soc. **227**, 1 (1987).
[58] H. A. Feldman, N. Kaiser and J. A. Peacock, Astrophys. J. **426**, 23 (1994).
[59] M. Tegmark, A. N. Taylor and A. F. Heavens, Astrophys. J. **480**, 22 (1997).
[60] A. Meiksin, M. White and J. A. Peacock, Mon. Not. Roy. Astr. Soc. 304, 851 (1999).
[61] M. White, Astropart. Phys. **24**, 334 (2005).
[62] H.-J. Seo and D. Eisenstein, Astrophys. J. **633**, 575 (2005).
[63] W. Hu, Phys. Rev. D **65**, 023003 (2002).
[64] W. Hu and B. Jain, Phys. Rev. D **70**, 043009 (2004).
[65] U. Seljak and M. Zaldarriaga, Astrophys. J. **469**, 437 (1996).
[66] D. Eisenstein, W. Hu and M. Tegmark, Astrophys. J. **518**, 2 (1998).
[67] M. Ouchi, K. Shimasaku, S. Okamura et al., Astrophys. J. **611** 660 (2004).
[68] S. Hannestad, astro-ph/0510582.
[69] S. Dodelson, A. Melchiorri and A. Slosar, astro-ph/0511500.
[70] A. D. Dolgov, Phys. Rep. **370**, 333 (2002).
[71] R. Scoccimarro, Phys. Rev. D **70**, 083007 (2004)
[72] K. Abazajian and S. Dodelson, Phys. Rev. Lett. **91**, 041301 (2003).
[73] Y. S. Song and L. Knox, Phys. Rev. D **70**, 063510 (2004).
[74] M. Fukugita, G.-C. Liu and N. Sugiyama, Phys. Rev. Lett. **84**, 1082 (2000).
[75] S. Wang, Z. Haiman, W. Hu, J. Khoury and M. Morgan, Phys. Rev. Lett. **95** 011302 (2005).
[76] F. Bernardeau, S. Colombi, E. Gaztanaga and R. Scoccimarro, Phys. Rep. **367**, 1 (2002).
[77] S. Matarrese, L. Verde and A. F. Heavens, Mon. Not. Roy. Astr. Soc. **290**, 651 (1997).
[78] L. Verde, A. F. Heavens and S. Matarrese, Mon. Not. Roy. Astr. Soc. **300**, 747 (1998).

[79] D. Dolney, B. Jain and M. Takada, Mon. Not. Roy. Astr. Soc. in press (astro-ph/0409455).

[80] A. F. Heavens, L. Verde, and S. Matarrese, Mon. Not. Roy. Astr. Soc. **301**, 797 (1998).

[81] A. E. Schulz and M. White, astro-ph/0510100.

[82] H. A. Feldmann, J. A. Frieman, J. N. Fry and R. Scoc-cimarro, Phys. Rev. Lett. **86**, 1434 (2001).

[83] L. Verde et al., Mon. Not. Roy. Astr. Soc. **335**, 432 (2002).

[84] D. Babich and A. Loeb, astro-ph/0509784.

[85] L. Verde, et al., Astrophys. J. Suppl. **148**, 195 (2003).